Intertidal Exposure Modulates Time-Integrated Heat Tolerance of the Eastern Oyster *Crassostrea virginica*

Andrew R. Villeneuve [*1], Brittany Jellison [1], and Easton R. White [1]

[1]Department of Biological Sciences, University of New Hampshire, Durham, NH 03824

Abstract

The rise of unprecedented heatwaves globally has caused an increase in mass mortality events, motivating the need for accurate predictions of population declines. Predicting organismal function under fluctuating thermal regimes is a central challenge in thermal biology, particularly in intertidal systems where organisms experience rapid shifts between submerged and aerial exposure. Here, we developed thermal death time (TDT) curves for the eastern oyster *Crassostrea virginica* under both immersed and emersed conditions to construct exposure-specific thermal tolerance landscapes (TTLs). Using heart rate monitoring to determine time to death, we found significant differences in thermal tolerance between immersion and emersion. At lower lethal temperatures, submerged oysters survived longer than oysters in air, but this relative tolerance flips at temperatures above 37 °C. We then integrated these TTLs into a dynamic survival model that accounted for tidal cycles, allowing us to predict cumulative survival of oysters in the intertidal zone. After calibrating the model to account for field acclimation, our model predictions corroborated the survival of oysters in the field, demonstrating the utility of exposure-specific TTLs in forecasting survival outcomes. Simulated warming of 2 °C in air, water, and both exposures revealed particular sensitivity of oysters to atmospheric heatwaves — survival dropped by 12.9 – 13.8% across modelled sites when only air temperatures were increased. Our findings highlight the importance of considering exposure type in thermal tolerance assessments and provide a framework for predicting organismal responses to thermal stress in fluctuating environments.

Keywords: thermal tolerance landscape, thermal ecology, heat failure, intertidal bivalves, mechanistic model, ecophysiology

1 Introduction

Climate change is warming the baseline over which extreme temperature pulses occur in both air and water, driving an increase in atmospheric and marine heatwave events globally (Harris et al., 2018; Hobday et al., 2018; Oliver, 2019; Xu et al., 2022). Environmental variability (or

*drew.villeneuve@unh.edu

weather) occurring over minutes to months, rather than gradual mean warming over decades, disproportionately drive biological responses because short-term variability more closely matches the timescale of organismal function and lifespans (Bailey and van de Pol, 2016; Bates et al., 2018; Sasaki et al., 2025; van de Pol et al., 2017). Indeed, some of the most apparent responses to ongoing anthropogenic warming are mass mortality events driven by extreme heatwaves, particularly in marine foundation species that cannot behaviorally thermoregulate (Smith et al., 2023; Smith et al., 2024; Wernberg et al., 2024).

The unprecedented rise of modern marine mass mortality events has made the use of correlative data approaches to predict their occurrence and extremity difficult, as analogous historical events are rare. Mechanistic ecophysiological models provide a method of determining biological responses to environmental variability (measured as body temperature), allowing for more direct quantification of the effects of a rapidly changing climate and weather system (Briscoe et al., 2023; Peterson et al., 2015). Traditional thermal performance metrics, whether derived dynamically or statically, are traditionally treated as thresholds that set a hard limit between organism persistence and death (Angilletta, 2009; Deutsch et al., 2008; Lutterschmidt and Hutchison, 1997). However, predicting when these mortality events will occur requires understanding not only the upper thermal limits organisms can tolerate, but also the duration over which exposure to extreme temperatures can be sustained before physiological failure occurs. Critically, these translation approaches have struggled to accommodate the temporal component of thermal exposure. The path towards organism death is not a sudden cliff, but is rather due to an accumulation of thermal injury as different molecular, cellular, and organismal processes fail to maintain internal homeostasis (Ern et al., 2023; Ørsted et al., 2022). Temperature stress through time can be conceived as a dose that results in predictable organismal impacts corresponding to the magnitude of temperature stress and its duration.

Given marine invertebrate mass mortalities have been attributed to extreme atmospheric and marine heatwave events, reconceiving of thermal tolerance as a time-integrated trait would advance our ability to predict biological responses. Recent advances in Thermal Death Time (TDT) curve models, also called Thermal Tolerance Landscapes (TTL) and Thermal Load Sensitivity (TLS), seek to describe the effects of lethal temperatures as a dose response (Arnold et al., 2025; Jørgensen et al., 2019; Rezende et al., 2014). These approaches describe a predictable response of organismal time to death over static temperature exposure. The underlying empirical survival likelihood functions (Rezende et al., 2020) or mortality rates (Jørgensen et al., 2021) can further be used to predict survival across variable temperature regimes by interpolating survival values into a continuous Thermal Tolerance Landscape (TTL; (Bullard et al., 2026); (Rezende et al., 2014)). TDT curves can vary in slope ('sensitivity') and intercept ('acute tolerance') across species (Alruiz et al., 2022; Jørgensen et al., 2021; Jørgensen et al., 2022; Rezende et al., 2014), ecotypes (Dwane et al., 2021), acclimation (Baeza Icaza et al., 2025; Castañeda et al., 2015), life stages (Truebano et al., 2018), and oxygen availability (Verberk et al., 2023). The TDT curve is ultimately an emergent phenomenon composed of multiple molecular, cellular, and organismal processes interacting at different timescales and temperature exposure to drive organism time to death (Arnold et al., 2025;

Bullard et al., 2026).

Dose frameworks like TTLs are thought to better describe thermal stress than static methods in highly variable environments like the intertidal zone (Dwane et al., 2021; Rezende et al., 2014). A key dimension influencing mortality risk in intertidal organisms is the cyclical alternation between aerial exposure and seawater immersion across tidal cycles, which imposes recurring and position-dependent thermal stress (Stillman et al., 2025). Many organisms in this harsh environment are well adapted to deal with temperature extremes, as well as concurrent stressors arising from desiccation, wave exposure, solar radiation, and shifts in water quality and oxygen availability. However, the heatwaves have accelerated the rate of catastrophic mortality events, such as the 2021 heat dome in the Pacific Northwest of the US and Canada that resulted in billions of dead organisms across a large geographic area (Hesketh and Harley, 2023; Raymond et al., 2022; Raymond et al., 2024; White et al., 2023). On short timescales, intertidal organisms can experience extreme and dynamic intertidal temperatures that make performance difficult to predict from the mean conditions alone (Denny, 2017; Dowd et al., 2015). Over longer timescales, organisms may accumulate plastic responses through prolonged exposure, seasonal acclimation (Dowd and Denny, 2020; Pereira et al., 2025) and variation across life stages (Deschamps et al., 2025; Dwane et al., 2025; Giménez, 2023). Rather than averaging over or removing this temporal component of variability to make inference easier, mechanistic models like TTLs emulate how organisms process varying temperature exposures and translate them into biological rates (Villeneuve and White, 2024). A pressing question is whether periodic immersion in the intertidal can buffer extreme emersion temperatures, and whether atmospheric or oceanic warming will be more impactful for intertidal organisms. Given the different stressors operating during low tide emersion and high tide immersion, it is not clear whether the TDT/TTL framework and dynamic survival models will accurately describe and predict intertidal stress accumulation.

Predicting when conditions result in mortality and quantifying the extent of mortality remain challenges to effectively forecast future mass mortality events in response to heatwaves. Here, we investigate the potential for exposure-dependent thermal sensitivity in intertidal populations of the eastern Oyster, *Crassostrea virginica* (Gmelin, 1791), using a thermal tolerance landscape approach. We first conducted static time to death assays for oysters in water (immersion) and air (emersion) exposures to determine if exposure type alters TDT shape. We then build a dynamic tolerance model that switches between thermal tolerance landscapes parameterized under different exposure scenarios depending on intertidal exposure and validate the model survival predictions against oyster field survival in Great Bay, New Hampshire, USA. We also use a simulation-based calibration of the dynamic tolerance model using field data to account for potential baseline differences in lab-held and field-deployed oysters. Finally, we explored the sensitivity of oysters across both exposure states to warming by calculating the rate of death (heat failure rates) and by adding 2 °C to measured intertidal water temperatures.

We hypothesize that different intertidal exposures (immersion or emersion) present unique physiological challenges that propagate at different rates under stressful temperatures, resulting in dif-

ferent underlying thermal death time curves. Namely, we expect oysters exposed to air will be more die faster than oysters submerged in water over low temperatures due to desiccation, but that at higher temperatures immersed oysters will persist for longer than emersed oysters due to metabolic depression during air exposure. Warming in air will be more deleterious to oyster survival than the same amount of warming in water due to the relatively smaller warming tolerance margin in aerially exposed oysters, despite the more rapid heat failure oysters experience in water. We further expect that our lab-parameterized dynamic tolerance model will slightly overpredict mortality of field oysters due to the acclimation potential of these oysters to variable intertidal conditions.

2 Materials and Methods

2.1 Organism Collection and Preparation for Experiments

We collected 400 adult NEH line diploid Eastern oysters (*Crassostrea virginica*) from Fox Point Oysters, an aquaculture site located in Great Bay, New Hampshire, USA (43°07'45.6"N, 70°51'03.6"W), for use in immersed and emersed thermal tolerance experiments in the summer and fall of 2024. We kept experimental oyster stock used for immersed experiments in a 300-liter flow-through circular tank with airstones, so that oysters were able to filter feed from the raw seawater. We kept experimental oyster stock in a 300-liter flow-through circular tank with airstones, so that oysters were able to filter feed from the raw seawater. Water temperatures in the flow-through CML seawater system averaged 14.7 °C (2.2 °C s.d.) during the experimentation period (May 9th-September 9th 2024). Oysters used in immersed experiments were acclimated in a 568-liter indoor recirculating seawater system for at least one week prior to experimentation, with a chiller setpoint of 15 °C (15.2 °C, 0.96 s.d.) to match the average acclimation temperature of oysters in the immersed TDT experiment.

We measured and weighed oysters selected for experimentation using an analytical balance and digital calipers. Average shell mass across immersed treatments was 40.9 g (7.0 g s.d.), and average shell height was 75.2 mm (7.4 mm s.d.), and in the emersed treatments the average shell mass was 20.0 g (4.8 g s.d.) with an average shell height of 61.0 mm (5.4 mm s.d.; Table S1). Because oyster sizes between experiments were different due to availability, we included size as a covariate in later models.

We used two ElectricBlue PULSE V2 (ElectricBlue CRL, Porto, Portugal) heart frequency loggers to amplify and record infrared signals from Vishay CNY70 optical infrared sensors (Vishay Intertechnology, Inc, Malvern, PA, USA). Infrared detection of heart beats relies on infrared (IR) light-emitting diode sensors with a dual emitter and phototransistor to record reflected light. By detecting changes in reflected light when positioned over a heart, the PULSE unit records the fluctuations as an electric signal for later processing (Abbas et al., 2024; Burnett et al., 2013; Levinton et al., 2020; Lima et al., 2025). PULSE units recorded data at 20Hz (5ms intervals). We used a rotary tool (WEN 23190, WEN Products, Elgin, IL, USA) with a sanding attachment to grind a hole directly above the heart in the left (cupped) valve, as the shell of *C. virginica* is

generally too thick to allow for sufficient IR transmission and reflection back to the sensor.

2.2 Submerged and Exposed Experimental Design

For the immersed experiment, we exposed oysters to chronic, static water temperatures in a flow-through experimental seawater system composed of ten 80L tanks equipped with a system-wide control system (APEX, Neptune Systems, Morgan Hill, CA, USA) to monitor and control water quality parameters through connected heat bars. We were limited to 20 oysters per experimental trial (10 in the case of our first submerged trial) due to the PULSE units having capacity for ten channels each (Table S5). Therefore, we conducted a series of sequential, time-blocked trials in order to obtain desired sample sizes. We ended the trial once all oysters had died (determined by both referring to heart rate data and manual manipulation of shells) across treatments.

For the emersed trial, we used a pair of heated incubation chambers (Insect Rearing Chamber IN03, Darwin Chambers, St. Louis, MO, USA) to create static aerial temperature treatments. We maintained mean humidity levels between 68-72% by filling a tray of reverse-osmosis freshwater at the bottom of each chamber. These humidity levels approximate intertidal humidity levels in Great Bay, which are between 50-90% (Cheng et al, unpublished data). We recorded chamber temperature and humidity levels with separate digital loggers and with probes in a glycol solution (GSP-6G, Elitech Technologies, San Jose, CA, USA; Fig. S14).

We placed ten oysters outfitted with infrared sensors connected to a PULSE heart frequency unit into a subtank (immersed) or chamber (emersed) and monitored them daily for signs of gaping and cessation of cardiac activity. We stopped the experiment once all oysters showed no signs of cardiac activity and continued gaping even after manipulation. Due to equipment limitations, we were only able to conduct experiments on two emersed temperatures concurrently, as opposed to up to five concurrent temperatures with the immersed experiment, Table S5). Additional methodological details are available in Appendix Supplementary Materials and Methods 1.

2.3 Field Mortality Data

To validate our survival predictions, we monitored field-deployed oysters at two local intertidal sites in the summer of 2025. *C. virginica* is found intertidally throughout the Great Bay estuary, often associated with rockweed (*Ascophyllym nodosum*) cover (McKown et al., 2025). We deployed 83 oysters between May 16th and September 10th at Brackett's Point ("bracketts", 40 oysters, 43°03'39"N 70°52'21"W) and between May 29th and September 9th at Jackson Estuarine Lab ("JEL", 43 oysters, 43°05'31"N 70°51'53"W) in Great Bay, NH. Both sites have established intertidal oyster populations. Field-deployed oysters were from the same source we used for TDT experiments and were of similar size to those used in laboratory TDT trials. We labeled individual oysters and measured shell height using calipers to the nearest mm. At both sites, we periodically (weekly-biweekly) checked each oyster for signs of mortality, indicated by gaping valves that did not close upon touch.

At Brackett's Point, we evenly spaced eight cupside-up oysters to five 30 cm square cement pavers affixed with two part epoxy (A-788 Splash Zone Epoxy, Pettit Paint, Greensboro, NC, USA). On one paver, we affixed a temperature logger (T7.3 Envlogger, ElectricBlue, Porto, Portugal) recording temperatures every 15 minutes (Fig. S15). Each paver was inserted into cages made with 12.7mm galvanized hardware cloth to exclude predators. We placed these cages at roughly 1m above mean lower low water (MLLW; calculated later to be 0.904m MLLW) in the upper intertidal zone.

At JEL, we used four replicate oyster aquaculture 18 mm mesh bags containing eight oysters each and one bag with 11 oysters (Fig. S16). This design differed from the experiment at Brackett's Point due to equipment availabilities at experiment start time. We again measured and labelled oysters in the same fashion as at Brackett's Point. We deployed these bags in the upper intertidal zone, approximately 0.5m above MLLW (calculated later to be 0.681m). Oyster bags were anchored into the substrate in the upper intertidal, along with a HOBO TidbiT MX (HOBO Data Loggers, Bourne, MA) recording temperatures every 15 minutes. We also deployed a water pressure logger (MX20L-04, HOBO Data Loggers, Bourne, MA) within one of the field oyster cages recording ambient pressure data every minute between May 19th and June 12th at JEL and June 18th and July 1st at Brackett's Point. This ambient pressure data, in combination with intertidal temperature, were used to score each temperature observation as immersed or emersed at both JEL and Brackett's Point (Appendix Supplementary Materials and Methods 4).

2.4 Data Analysis

2.4.1 Tank Temperature and Dissolved Oxygen

We used mean water temperature as recorded by the Apex system probe or a temperature logger. The summary statistics for temperatures obtained with other data sources are found in the supplementary material (Table S6). To determine if dissolved oxygen changed across temperature treatments and with death, we calculated the 90th and 10 percentiles of dissolved oxygen to represent the approximate values when oysters entered experiment and when oysters died (most oxygen consumed; Table S7). We used a linear model to test for differences in dissolved oxygen across temperature treatments, and a one-way ANOVA to test for differences in dissolved oxygen between the 90th and 10th percentiles. This and all following analyses were conducted in R (v. 4.3.3).

2.4.2 Cardiac Activity Analysis

We conducted wavelet analyses of heart beat activity for each oyster on hourly timesteps using the `WaveletComp` package (Roesch and Schmidbauer, 2018). We extracted time to death for individual oysters by manually inspecting hourly wavelet plots for cessation of heartbeat activity. We used 15-minute intervals as our standard for time to death precision. We discarded nine oysters from analysis because the heartbeat was not apparent at any time during the spectral analysis. In the supplementary material (Appendix Supplementary Materials and Methods 3), we provide

further methodological details and examples of wavelet heartbeat spectral plots, raw heart beat signal, and resultant time to deaths.

2.4.3 Oyster TDT Model

To model oyster thermal death time, we examined our time to death data with generalized linear mixed effects models to examine variation arising from experiment dates, oyster size (mass, grams), exposure type, and assay temperature in a model-selection framework. Prior to constructing linear models of oyster time to death, we tested if oyster shell sizes were significantly different between field sites and field/lab experiments using one-way ANOVAs and Estimated Marginal Means (EMMs) averaged over sites and experiments obtained from the `emmeans` package (Lenth et al., 2025). We used total wet mass (g) and height (mm) of individual oysters as a proxy for size. Exploratory analysis found no differences in body mass (Type II one-way ANOVA, $\chi_8 = 6.09$, $P = 0.637$), or shell height (Type II one-way ANOVA, $\chi_8 = 7.298$, $P = 0.505$) across temperature treatments in lab experiments, but oysters used in the immersed experiments were significantly larger and heavier than those used in the emersed experiments (Type II one-way ANOVA, $\chi_1 = 95.095$, p = <0.001; Table S4). Therefore, we provided mass as a term in some of our candidate models to ensure mass did not explain significant variance in time to death residuals.

Once we established the inclusion of mass and the ability to remove the acclimation temperature term (Appendix Supplementary Materials and Methods 2), we proceeded constructing candidate additive and interactive models (Table 1). We used the corrected Akaike's information criterion (AICc) to examine support for the most parsimonious models, with a cut-off of ΔAICc < 2 (Burnham and Anderson, 2002). We first compared AICc values between a basic linear model (log10(time to death) temperature x exposure) and a model with experiment as a random intercept (log10(time to death) temperature x exposure + (1|experiment)) using the `lme4` package (Bates et al., 2015). Based on a lower AICc value for the basic model and the small variance explained by experimental trial (0.008), we elected to drop this random effect from model exploration. Data residuals across candidate models were all normally distributed (Shapiro-Wilk test, $P > 0.05$).

To calculate thermal death time parameters, we used the best-supported model as the basis for the `tolerance.landscape` function developed by Rezende et al. (2014, 2020). This function calculates the acute thermal tolerance parameter $CT_{max(1min)}$ as the x-intercept ($\log_{10}(t) = 1$ min) of the semilogarithmic TDT curve and the chronic thermal tolerance parameter z as the slope of the relationship between assay temperature (T_{assay}) and log10-transformed time to death (t) (Equation (1)). We also calculate CT_{max} at a duration of 1 h ($CT_{max(1h)}$) to derive a more biologically relevant measure of thermal tolerance equivalent to single-threshold thermal tolerance metrics (Jørgensen et al., 2021).

$$\log_{10}(t) = \frac{(CT_{max(1min)} - z)}{T_{assay}} \tag{1}$$

We propagated error around the slope and intercept parameters from each linear model within

the `tolerance.landscape` function to calculate standard error around the z (1/slope) and $CT_{max(1min)}$ (-intercept/slope) parameters. We estimated the error using first-order Taylor series expansion via the Delta method. We used the variance around the slope term alone to calculate the error around z. To calculate error around $CT_{max(1min)}$, we needed to propagate uncertainty in both intercept and slope, requiring calculation of a covariance matrix and mixed partial derivatives.

2.5 Heat Failure Rates

Heat failure rates provide a thermodynamically informed measure of how sensitive a physiological rate (in this case, time to death) is to increasing temperature. Converting thermal tolerance to heat failure rates aligns this response to how metabolic scaling is typically understood (Dell et al., 2011; Jørgensen et al., 2022; Payne et al., 2025; Stark et al., 2025). This translation allows for the application of scaling theory to understand how different stressors may or may not have predictable effects on thermal tolerance, which has not been adequately explored. To determine how sensitive oyster death rates are to temperature and situate our results against other time to death data in mollusks, we calculated the heat failure rate of *C. virginica* from the empirically derived TDT curves using an Arrhenius analysis of activation energies, and compared these rates against values from a previous meta-analysis supplemented with values from the literature ((Jørgensen et al., 2022)). The slope β of the relationship between the log of heat failure rate (1/time to death, min) and 1/temperature (in Kelvin) results in a scaling parameter of heat failure sensitivity. The Arrhenius activation energy, which provides a thermodynamic measure of temperature effects on heat failure, can then be calculated:

$$E_a = \frac{-R\beta}{N_a C} \tag{2}$$

Where R is the molar gas constant (8.31 J $K^{-1}mol-1$), N_a is Avogadro's constant (6.022×1023 mol^{-1}), and C is a unit conversion factor into electrovolts (eV) (1.602 × 10-19 J eV^{-1}). A low E_a ($\approx$0.66 eV) is common in permissive-range, monotonic models of biological rates as described in the Metabolic Theory of Ecology (MTE), such as metabolic rate (Brown et al., 2004; Dell et al., 2011; Michaletz and Garen, 2024; Sibly et al., 2012). Higher E_a values are common in the descending portion of unimodal TPCs (Arnoldi et al., 2025; Michaletz and Garen, 2024), and exceed 4 eV up to 20 eV for steep TDT curves (Jørgensen et al., 2022). By calculating activation energy, we can also determine Q_{10}, a measure of the factorial change in rate over a change of 10 K and is a more common cognate of Arrhenius activation energy E_a (Q_{10} between 2-3 is typical for monotonic metabolic rates, and exceeds 1,500 for lethal TDTs). Following methods outlined by (Jørgensen et al., 2022), we calculated the Q_{10} of thermal death time curves as:

$$Q_{10} = e^{\frac{10KE_a}{k_b T^2}} \tag{3}$$

Where E_a is the activation energy for heat failure, k_b is Boltzmann's constant (8.617×10-5

eVK^{-1}), and T is a chosen temperature from which Q_{10} is calculated. We chose 307.91 K (34.76 °C) as the mean assay temperature in our expanded dataset of mollusk thermal death time experiments (Jørgensen et al., 2022).

2.6 Field Mortality Prediction with Intertidal Dynamic Survival Model

We extended our analysis of *C. virginica* time-dependent thermal tolerance to the creation of an intertidal dynamic survival model (Villeneuve and White, 2024). This model integrates two thermal tolerance landscapes we parameterized for low tide (emersed) and high tide (immersed) oysters. To simulate error around our predictions, we bootstraped time to death data to create 100 TTLs based on the original data. We further collected field data on oyster mortality in the upper intertidal to validate the predictions of this intertidal dynamic survival model against empirical data. To ensure the oysters used in field deployments were similar in size to those used in laboratory TDT experiments, we compared shell height across field and lab oysters using estimated marginal means (EMMs) from a linear model with site (Brackett's Point, JEL, Lab Immersed, Lab Emersed) as a fixed effect.

2.6.1 Temperature Logger Immersion

We determined the tide height and immersion history of the field mortality temperature logger relative to the Squamscott River tide gauge (NOAA 8422687; Section Supplementary Materials and Methods 4). We determined the temperature logger at JEL and Brackett's Point to have a height of 0.681 m and 0.904 m, and a time offset from the reference tide station of 17 and 6 minutes, respectively (Fig. S17). From these tide heights, we reconstructed the immersion status of each time point from the intertidal temperature logger time series. We interpolated our field temperature data from 15min to 1min resolution using linear interpolation to match the time resolution of the pressure data, providing a time series of field temperature and exposure type at one-minute intervals at both JEL and Brackett's Point.

2.6.2 Implementation of the Intertidal Dynamic Survival Model

Rezende *et al.* (Rezende et al., 2020) developed a numerical algorithm to predict mortality through time given a temperature time series and a thermal tolerance landscape (TTL). The method iteratively shifts a survival probability function, defined by the TTL, in response to temperature fluctuations and calculates instantaneous mortality at each time point. Total mortality is the cumulative sum of all of these mortality rates. However, in order to account for organism recovery that occurs after exposure to stressful temperatures, the total stress must be 'reset' at some interval (in terrestrial systems, every night), and the total survival over multiple resetting periods is calculated as the cumulative sum of survival fractions at the end of each day.

We adjusted the `dynamic.landscape` model developed by (Rezende et al., 2020) to both integrate TTLs from immersed and emersed oysters and reset stress at the end of each tidal cycle

in our new function `dynamic.landscape.2curve`. This function conditionally uses one of the two provided TTLs based on a temperature observation (emersed or immersed) to calculate heat stress at a given timestamp. We first broke up the temperature time series by tidal cycle, defined as starting with immersion ("immersed" status) and ending with the last emersed observation after a cycle of submersion and exposure occurs (Fig. 1A-B). Using experimentally-derived TTLs for immersed and emersed oysters (Fig. 1C-D), we allowed stress to accumulate starting from the first observation of submersion and ending with the last emersed temperature of the tidal cycle, thus effectively resetting stress every tidal cycle. Once the function finishes calculating the minimum survival $S_{min,TTL1}$ during the immersed period of the tidal cycle j, it switches to using the emersed TTL to calculate minimum emersed survival $S_{min,TTL2}$, but continues the time shift started at the beginning of the tidal cycle (Equation (4)).

$$S_j = S_{min,TTL1} - (100 - S_{min,TTL2}) \tag{4}$$

This allows stress to carryover from submersion. To calculate cumulative mortality over the length of entire tide series (n), we calculated the final cumulative sum of mortality S_{final} across both immersed and emersed exposures for each tidal cycle j (Equation (5)).

$$S_{final} = 100 \times \prod_{j=1}^{n} (\frac{S_j}{100}) \tag{5}$$

To parse the proportion of mortality occurring during tidal cycle submersion and exposure, we summed *log*-transformed mortality across tidal cycles (Fig. 1E). This *log* transformation accounts for the multiplicative nature of survival over time, allowing additive comparisons across tidal cycles and enabling attribution of cumulative mortality to each condition. In addition to calculating total survival over the temperature time series across both field sites, we also calculated survival using just a single TTL (immersed or emersed) for all tidal cycles to examine the relative importance of each exposure type to total mortality.

To establish prediction goodness-of-fit, we first calculated a percent change analysis of field and predicted survival data based on field survey dates. From this percent change analysis, we then calculated Root Mean Square Error (RMSE) between model predicted survival and observed survival at each field site. We also calculated Kaplan-Meier survival estimates for each field site using the `survival` (Therneau et al., 2026) package to calculate the 95% Confidence Interval of field observed survival probability. At JEL, we observed two extreme mortality events on July 18th and 24th, 2025 that did not correspond with extreme temperature events in our intertidal logger data. Construction at the marine station dock occurred during this time period. Therefore, we conducted an analysis both including (results in Section Supplementary Materials and Methods 2) and excluding (results in main text) these two mortality events from our goodness-of-fit analysis, as they likely represent non-thermal stressors.

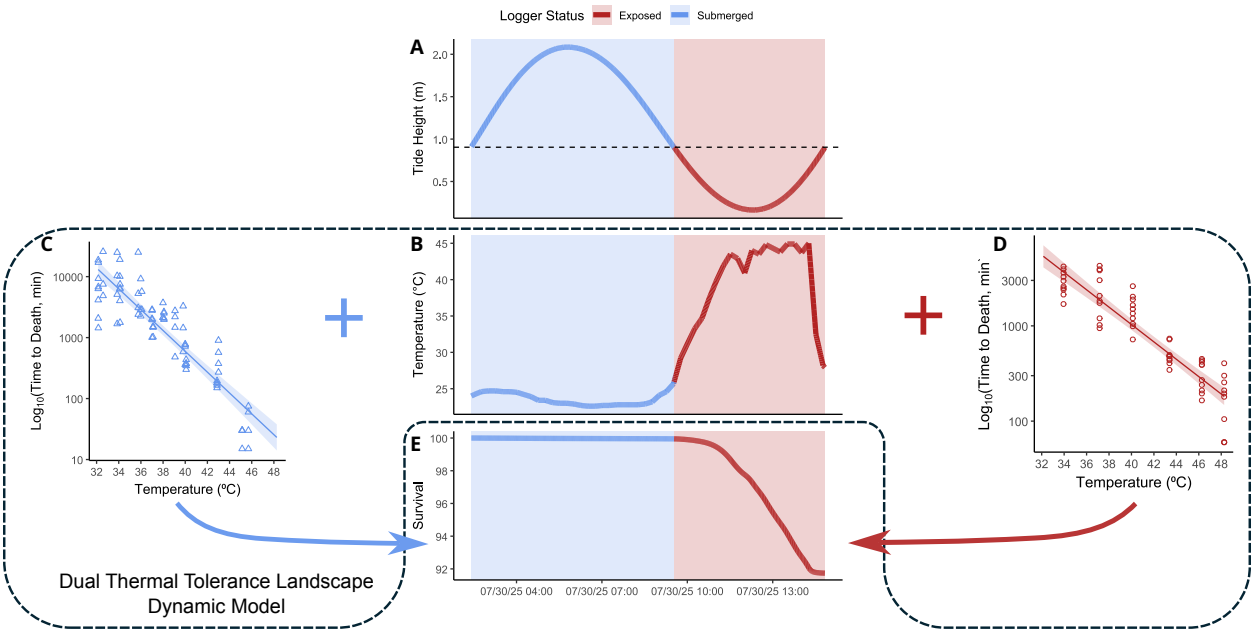

Figure 1: Conceptual figure of predicting survival in the intertidal eastern oyster *Crassostrea virginica* in a single tidal cycle. A tide cycle is defined as starting with immersion and ending immediately after a full immersion-emersion cycle. A) A tidal height time series and corresponding temperature logger tide height are used to delineate periods of submersion and exposure (immersion and emersion). B) These periods of logger submersion are converted to an exposure status for observed intertidal temperature taken from a data logger. C) and D) represent the thermal death time (TDT) curves for oysters submerged in water (immersion at high tide, blue) and exposed to air (emersion at low tide, red). These curves are then used as the basis for a probabilistic Thermal Tolerance Landscape (TTL) for each exposure type. E) Each exposure TTL is then used to calculate cumulative survival conditionally based on the exposure status of each temperature observation. We finally calculate the survival of oysters across multiple tide cycles to produce a prediction of cumulative survival over time in the intertidal.

2.6.3 TDT Bootstrapping

To quantify error around our modeled survival estimates, we used a nonparametric bootstrap procedure to resimulate thermal tolerance landscapes for each of the two exposure types 100 times, and then predict survival over field temperatures using these 100 landscapes. We resampled the empirical residuals of each time to death experiment with replacement, stratified by temperature, to match the original sample size we used in each experiment. This resampling procedure maintains the original statistical structure of the time to death data while allowing for variability in slope and intercept estimates. We then refit the linear models to each resampled dataset and recalculated thermal tolerance landscapes using the `tolerance.landscape` function, resulting in 100 bootstrap thermal tolerance landscapes. We then used our custom `dynamic.landscape.2curve` function to predict survival over the field temperature time series using each of the 100 bootstrap thermal tolerance landscapes for both exposure types.

2.6.4 TDT Curve Simulation-Based Calibration

Exploration of average field acclimation temperature data revealed that oysters used in TDT experiments were exposed to mean intertidal acclimation temperatures (mean immersed oysters 14.7 °C, 2.2 °C s.d., mean emersed oysters 15.2 °C, 0.96 °C s.d.) with average water temperatures at JEL and Brackett's Point calculated from intertidal loggers (two week post-deployment mean water temperatures, mean JEL 16.32 °C (2.29 °C s.d.), mean Brackett's Point 17.28 °C (1.63 °C s.d.). However, intertidal air temperatures were warmer and much more variable (JEL 19.07 °C 7.47 °C s.d. and Brackett's Point 19.46 °C 6.29 °C s.d.), indicating field oysters may have become acclimated to both variable and warmer exposure conditions. Therefore, we completed a sensitivity analysis to see how manipulating TDT curve parameters based on hypothetical acclimation to warmer temperatures would affect our predicted survival results. We chose two larger $CT_{max(1min)}$ values and two smaller z values in addition to the original calcualted values. This is based on research in *Drosophila* and the oyster *Magallana gigas* that show acclimation to warmer temperatures tends to increase $CT_{max(1min)}$ and decrease z (Baeza Icaza et al., 2025; Rajagopal et al., 2005). These authors found warming acclimation increased $CT_{max(1min)}$ by about 2-3 °C and decreased z by about 2, or did not reduce z at all. Based on the behavior of these parameters, we bootstrap simulated the survival over field temperatures again, but this time varying the slope (z and $CT_{max(1min)}$) and intercept (z) across all possible combinations, for a total of 18 new TTLs (all combinations of 3 candidate z and $CT_{max(1min)}$ values per curve equals 9 parameter sets per immersed/emersed exposure, with a total of 81 unique combinations; Fig. S18). Similar to the bootstrapping simulation procedure used to resimulate the original two TTLs, we resimulated the data by resampling with replacement the empirical residuals, but over TDT curves with one of the 18 possible slopes and intercepts. We then recalculated survival through time of oysters at JEL and Brackett's Point using intertidal logger temperature data, and the difference in survival between field survival census dates calculated for both field and candidate predicted survival data. From this percent change analysis, we calculated model prediction goodness of fit with Root Mean Square Error (RMSE) for each

candidate TTL combination. We identified the immersed and emersed TDT parameter combination that minimized RMSE across candidate parameters as a possible field acclimation-optimized model.

2.6.5 Warming

To determine the relative importance of future air and water temperature warming to field oyster survival, we simulated future temperature scenarios by adding +2 °C to either air temperatures during emersed periods only, water temperatures during immersed periods only, or both air and water temperatures simultaneously. We then used the optimal selected TDT curve parameters from the simulation-based calibration step as the basis of the TTLs used to predict survival under these future warming scenarios.

3 Results

3.1 Thermal Death Time Curves and Thermal Tolerance Landscapes

Under model selection the best-supported model modeled time to death as an interactive function of treatment temperature and experiment exposure type (Table 1). We found strong support for the interactive effect ($P = 0.003$) of temperature and exposure type on time to death (Gaussian Linear Mixed Effects Model, $F_{3,136} = 194.6$, $R^2 = 0.811$). The model predicted time to death to decrease significantly with increasing temperature ($P < 0.001$). The slope of the immersed TDT curve (β = -0.171) was significantly steeper than the slope of the emersed TDT curve (β = -0.091, $P < 0.001$), indicating that while immersed oysters were more tolerant than emersed oysters at lower temperatures, immersed oysters accumulated heat stress faster than emersed oysters as temperature increased (Table 2).

Model	K	AIC_c	ΔAIC_c	AIC Weight	Log Likelihood
$\log_{10}(min.of.death) \sim temp \times exposure$	**5**	**66.13**	**0**	**0.95**	**-27.84**
$\log_{10}(min.of.death) \sim temp \times mass_g \times exposure$	9	72.07	5.95	0.05	-26.34
$\log_{10}(min.of.death) \sim temp + mass_g \times exposure$	5	105.86	39.73	0	-47.71
$\log_{10}(min.of.death) \sim temp + exposure$	4	107.21	41.09	0	-49.46
$\log_{10}(min.of.death) \sim temp + mass_g + exposure$	6	107.99	41.86	0	-47.68
$\log_{10}(min.of.death) \sim temp$	3	115.6	49.48	0	-54.71

Table 1: Model selection outputs for TDT experiments. Bold face font indicates model selected for ultimate analysis.

While we did not record tank-specific oxygen concentrations for each oyster, and thus omitted this as a model term, our analysis indicates that dissolved oxygen (DO) levels, represented by the 90th and 10th percentiles, did not significantly vary across temperature treatments. DO at the 90th percentile (Linear Model, $P = 0.822$) and the 10th percentile (Linear Model, $P = 0.617$) remained

	Estimate	Standard Error	t-value	P value
Intercept	6.662	0.324	20.590	**<0.001**
Temperature (°C)	-0.091	0.008	-11.788	**<0.001**
Immersed Exposure	2.949	0.453	6.503	**<0.001**
Emersed Exposure	-0.080	0.011	-7.015	**<0.001**

Table 2: Linear model summary of the immersed and emersed experiment TDT models ($\log_{10}(min.of.death) \sim temp \times exposure$). Bold font indicates P values < 0.05.

consistent between treatments, suggesting similar maximum and minimum DO levels. However, a One-way ANOVA revealed that the 10th percentile of DO was significantly lower than the 90th percentile across all temperature treatments ($P < 0.001$), indicating a marked reduction in DO as oysters neared mortality. These findings suggest that oxygen dynamics may have contributed to thermal tolerance across all temperature conditions.

We calculated the acute thermal tolerance parameter $CT_{max(1min)} = 56.24$ °C $\pm$ 5.38 (-intercept/slope $\pm$ SE), the biologically realistic tolerance at one hour exposure $CT_{max(1hr)} = 45.83$ °C, and a thermal sensitivity parameter $z = 5.85 \pm 0.33$ (-1/slope $\pm$ SE) for the immersed oyster TDT. For the emersed oyster TDT, we calculated comparatively larger parameter values of $CT_{max(1min)} = 73.05$ °C $\pm$ 6.87, $CT_{max(1hr)} = 53.55$ °C, and $z = 10.97 \pm 0.66$ (Fig. 2). While the interactive model explained 81.1% of the variance (adjusted $R^2 = 0.811$), TDT curves calculated for each exposure explained slightly more variance (emersed $R^2 = 0.83$, immersed $R^2 = 0.8$). Above 37.03 °C, where these two TDT curves intersect, oysters that were emersed in air could withstand elevated temperatures longer than when in an equivalent water temperature. Below 37.03 °C, oysters in water could withstand lethal temperatures longer than oysters in air.

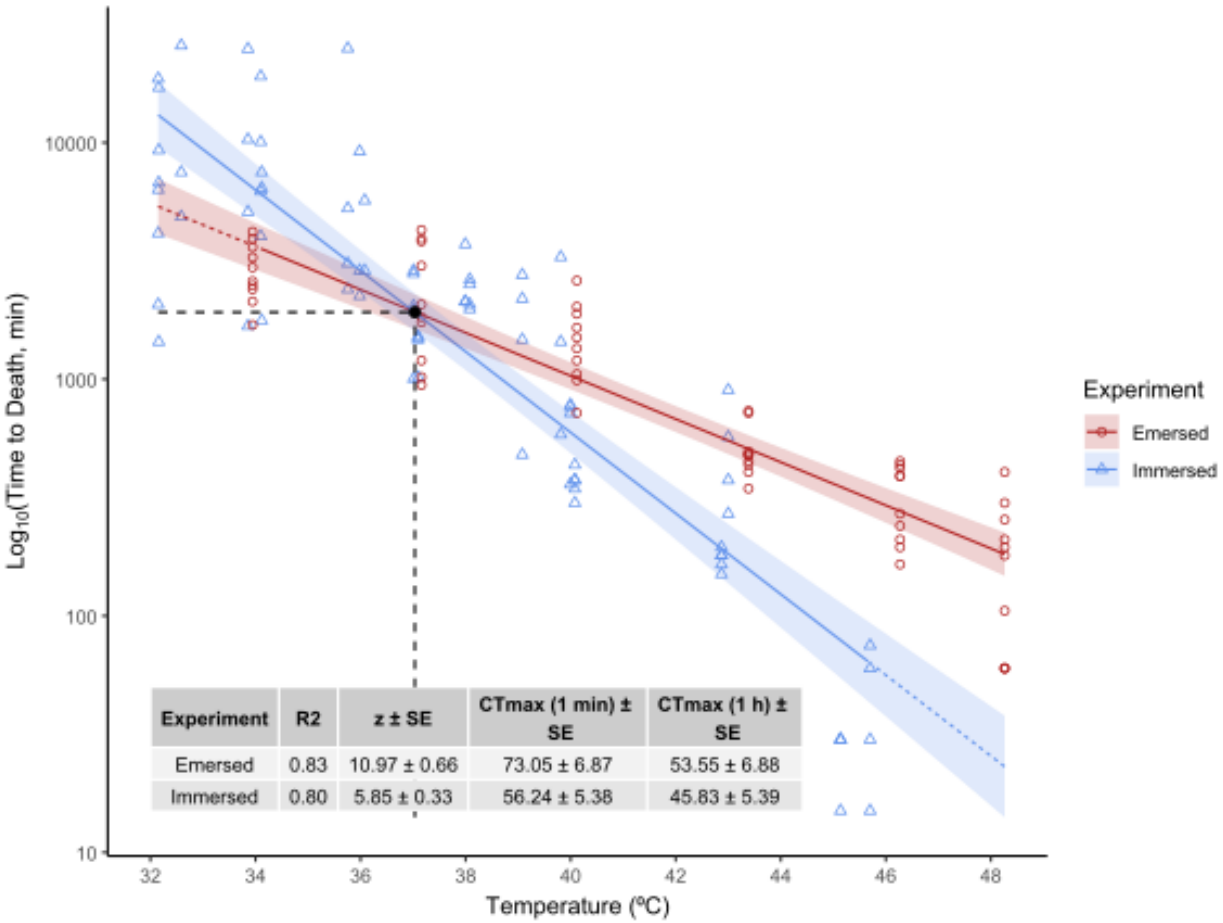

Figure 2: Thermal Death Time (TDT) curve for adult *C. virginica* exposed to air and water immersion heat stress. Thermal Death Time (TDT) curve for adult *C. virginica* exposed to air and water immersion heat stress. Ribbons around lines of fit are confidence intervals. Dashed line of fit describes the model when extrapolated beyond bounds of time to death data collected. Inset table contains TDT parameters, including R^2 (goodness of fit between the parameterized TDT curve and raw data), CT_{max} (acute thermal tolerance, x intercept when y = 1 min), and z (chronic thermal tolerance, slope of line). Standard error around CT_{max} and z were propagated with Taylor series expansion via the Delta method from linear model fit parameters (see Methods). The black point and dashed lines indicate the point of TDT curve intersection at 37 °C and 1,941 minutes.

3.2 Heat Failure Rates

We calculated the activation energy for heat failure as 3.283 eV and a Q_{10} of 55.57 for immersed *C. virginica*, and an activation energy of 1.78 eV and Q_{10} of 8.86 for emersed *C. virginica*, indicating emersed oysters are much more temperature sensitive than immersed oysters. This failure rate is well within the distribution of previously calculated values for mollusks (45.16% percentile and 9.68% percentile, immersed and emersed, Fig. S19). However, these values indicate that heat failure was not as rapid in *C. virginica* as other species, further confirmed by the relatively high

z values (5.85 and 10.97 for immersed and emersed oysters, respectively). Emersed oysters are therefore less effected by heating than immersed oysters, and generally *C. virginica* is a resilient mollusk species to warming.

3.3 Field Validation of Intertidal Dynamic Survival Model

Oysters used in the field experiments were not significantly longer than those used in the TDT lab experiments (EMM ± SE: field = 68.7 ± 1.6 mm, experiment = 68.6 ± 0.90 mm, $P = 0.94$). Oyster height was not different between field sites (EMM ± SE: Brackett's Point = 68.7 ± 1.7 mm, JEL = 68.8 ± 1.8 mm, $P = 0.9$).

Intertidal temperatures at our field sites had mean values of 21.4 °C (5.52 °C s.d.) at Brackett's Point and 20.5 °C at JEL (4.51 °C s.d.), maximum values of 48.0 °C at Brackett's Point and 42.3 °C at JEL (August 12th and July 16th 2025, respectively), and minimum values of 8.4 °C at Brackett's Point and 7.7 °C at JEL (May 23rd and June 3rd, 2025, respectively; Fig. 3A). The distribution of immersed water temperatures closely approximated that of water temperature recorded from a nearby NERRS buoy, but had more extreme high temperature values (Fig. S21). This is an artifact of cooling loggers at the start of immersion, indicating body temperatures of oysters may be high at the start of immersion tidal cycles. Emersion temperature distributions were wider, reflecting relatively cool nighttime and cloudy day air temperatures as well as extremely hot conditions during sunny daytime conditions.

Of the 83 oysters we deployed across two deployments, 42 oysters died (6 at Brackett's Point, 36 at JEL). We did not observe any evidence of predation from crabs or oyster drills on our deployed oysters. Our intertidal dynamic survival model predicted survival of 22.29% (7.7, 22.7 95% CI) for oysters deployed at Brackett's Point, and 47.22% (36.4, 58.3 95% CI) for oysters deployed at JEL. These predictions are respectively lower and higher than field observed values of 85% at Brackett's Point and 16.28% at JEL (26.2% and 290% of modeled survival (Fig. 3B), and bootstrapped final survival values did not overlap with any field observations (Fig. S20).

Our method predicted higher survival at all time points compared to models that use just an immersed or emersed-parameterized dynamic tolerance model. In the dual-TTL model, we attributed 99.3%/89% (Brackett's Point/JEL) and 0.7%/11% (Brackett's Point/JEL) of modeled mortality to emersed and immersed periods of tidal cycles during the field deployments, respectively (Fig. S22). Overall, the model performed best at Brackett's Point (RMSE = 6.4, 95% CI = 5.57/6.71) compared to JEL (RMSE = 10.4, 95% CI = 10.36/10.47; Fig. S23).

3.4 Simulation-Based Calibration of the Dynamic Tolerance Model

Our calibration analysis of TTL parameter combinations revealed an optimal combination of $CT_{max(1min)}$ and z values for both immersed and emersed oysters that minimized RMSE between predicted and observed survival at both field sites (Brackett's Point = 0.93, JEL = 2.29; Figure 3.4). For the emersed TTL at Brackett's Point, increased $CT_{max(1min)}$ and reduced z $CT_{max(1min)} = 74.2$ °C, $z = 8.3$) minimized RMSE, while at JEL the original $CT_{max(1min)}$ and z parameters minimized

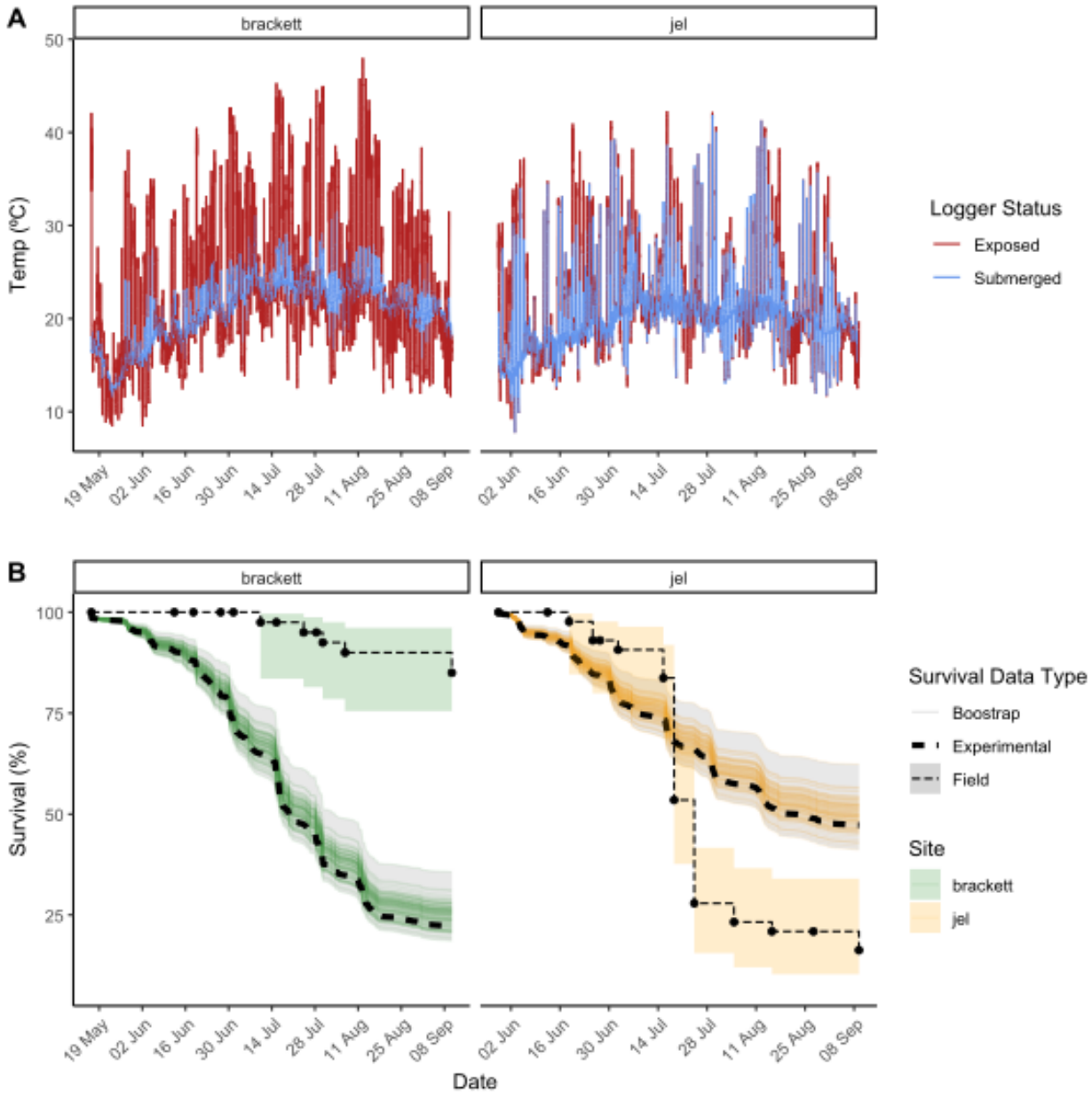

Figure 3: Intertidal temperatures at Brackett's Point and JEL, with corresponding observed and modeled survival under original TTLs. A) Intertidal temperature in the upper intertidal of Brackett's Point between May 16th and September 10th 2025 (left panel) and Jackson Estuarine Lab (JEL; right panel) between May 29th and September 9th 2025, co-located with oyster mortality survey. Red portions of the time series indicate time stamps when the loggers (and by proxy, the field deployed oysters) were predicted to be above water (low tide, exposed status), blue portions when loggers were predicted to be below water (high tide, submerged status). B) Field observed survival (points), 95% CI of field survival (colored ribbon), and modeled survival of 83 oysters distributed across Brackett's Point and JEL. The line type indicates the type of survival prediction, with the dashed line representing field survival, the dotted black line the survival prediction given by the experimental data, and the multiple solid lines indicating the 100 bootstrapped survival predictions from the original survival model.

RMSE $CT_{max(1min)}$ = 73.5 °C, z = 10.4). When the two extreme mortality observations at JEL from July 18th and 24th, 2025 are included, RMSE for the best fit combination of parameters $CT_{max(1min)}$ = 77.5 °C, z = 12)) rose to 10.34. For the immersed TTL at Brackett's Point, the original parameters $CT_{max(1min)}$ = 56.7 °C, z = 6) minimized RMSE, while at JEL a slightly larger $CT_{max(1min)}$ and lower z minimized RMSE $CT_{max(1min)}$ = 57.7 °C, z = 4.9; Fig. S24). Using these optimized TTL parameters, the intertidal dynamic survival model predicted survival of 83.9% for oysters deployed at Brackett's Point, and 68.2% for oysters deployed at JEL. These predictions are closer to field observed values of 85% at Brackett's Point and 16.28% at JEL (101.3% and 23.87% of modeled survival for Brackett's Point and JEL, respectively.

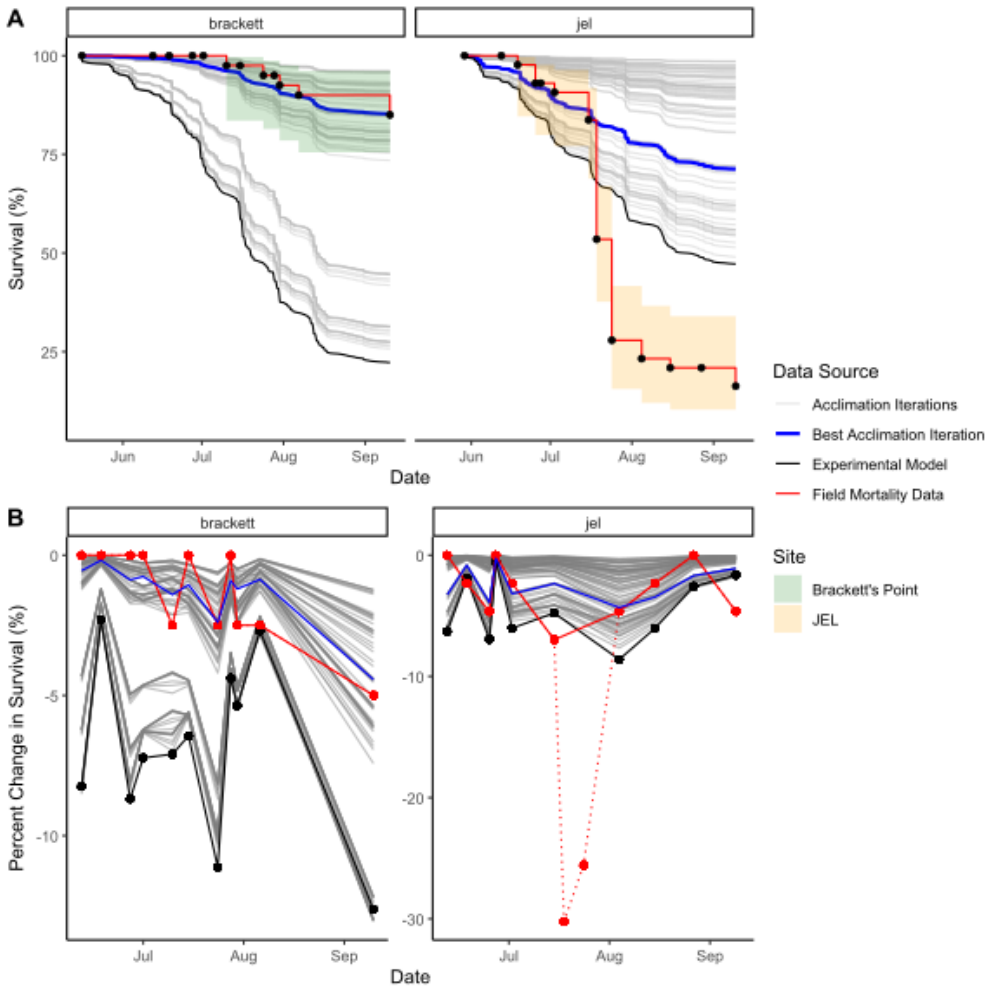

Figure 4: Survival predictions using simulation calibrated TTLs. A) Survival predictions produced from 81 different TTL parameter combinations (gray), with the best-fit model to field data (red) highlighted in blue. The colored ribbons indicate the 95% confidence interval around percent change in field survival. Modeled survival prediction using experimentally-derived TTLs shown in black. B) Percent change analysis used to identify the optimal combination of TTL parameters to minimize Root Mean Squared Error between predictions (gray lines) and field data (red lines and points). Black lines and points indicate modeled survival using experimentally-obtained TTLs. The percent change in survival given by the combination of TTL parameters that minimized RMSE are shown in blue. For field data from JEL, the two extreme mortality observations that were not attributable to heat stress and removed from percent change analysis and the final selection of the optimal TTL parameter combination are shown in dotted red lines.

3.5 Climate Warming Simulation

Under 2 °C of warming in both air and water applied to the intertidal temperatures, our model predicted the highest reduction in survival at both Brackett's Point and JEL (-20.8% and -37.2% change from 2025 baseline and end survival of 66.4% and 42.8%, respectively; Fig. 5) using the calibrated TTLs for each site. Warming in just air (Brackett's Point = -13.8% change, survival

= 72.3%, JEL = -30.9% change survival = 47.1%) resulted in more slightly mortality than just warming in water (Brackett's Point =-12.9% change, survival = 73.1%, JEL = -21% change, survival = 53.9%). While Brackett's Point was a hotter site, survival was higher than at JEL because we used the optimized TTL from the simulation calibration procedure, which possibly arose because of different heat hardening acclimation at the two sites.

Temperatures during emersion were clearly causing the accumulation of heat stress, while water temperatures at both sites were both much cooler than those necessary to result in significant accumulation of mortality. Slightly more elevated mortality at JEL during water warming scenario is attributable to the less precise parsing of whether a temperature observation occurred during tidal immersion or emersion (see Methods).

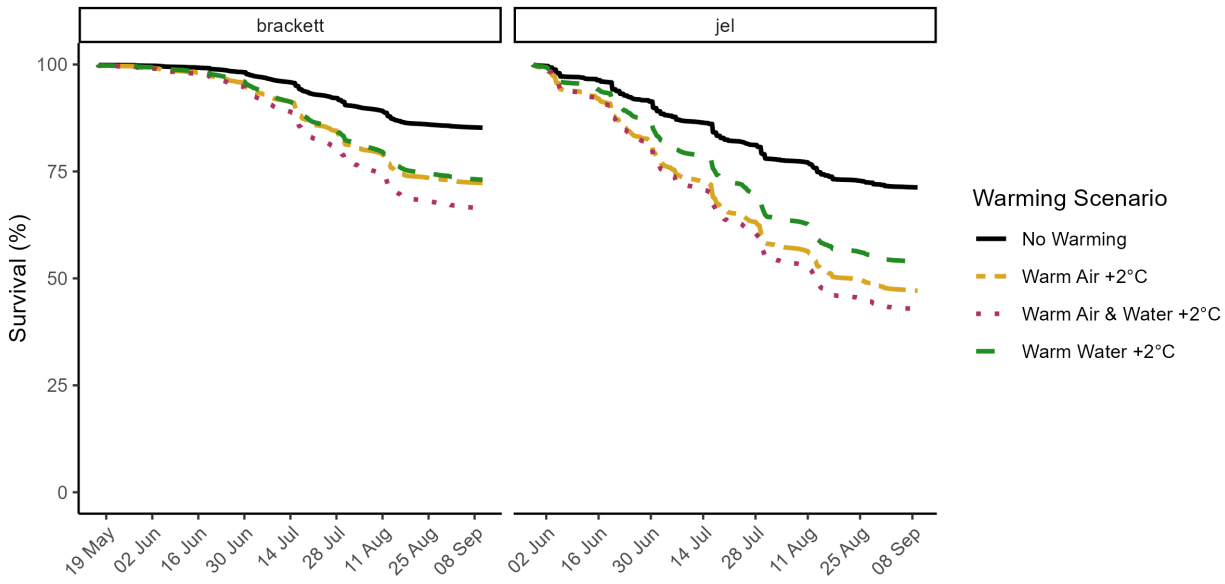

Figure 5: Impacts of 2° C warming on modeled intertidal oyster survival. Impacts of 2 °C warming during tidal emersion (yellow), immersion (green), and throughout the tidal cycle (red) on predicted oyster mortality at Brackett's Point and JEL. Warmer water had the smallest impact on oyster survival, with warming in both air and water having the largest impact on survival due to the relatively larger contribution of warmer emersion to mortality.

4 Discussion

Marine and atmospheric heatwaves pose a serious threat to persistence of intertidal invertebrates populations, but producing predictions of lethality has been hampered by a lack of generalization across heat events and changing exposure. Our results suggest that while *C. virginica* can withstand high temperatures for short periods of time, the accumulation of heat stress during low tide exposure can lead to rapid mortality. Our field validation of the intertidal dynamic survival model suggests that this model is a useful tool for predicting mortality in intertidal environments, but that further refinement is needed to account for the complex dynamics of biological stress accumulation, recovery,

and acclimation in the intertidal zone.

4.1 Thermal Death Time Curves Reveal Divergent Responses of Intertidal Thermal Tolerance

We found that emersed oysters persisted at higher temperatures longer than immersed oysters, and vice-versa at lower temperatures. This suggests that oyster tolerance mechanisms (whether physiological and/or behavioral) change in strength during tidal cycles (Fig. 6). We obtained dramatically larger values of $CT_{max(1min)}$ and z ($CT_{max(1min)} = 73.05$, $z = 10.97$ for emersed oysters than immersed oysters, indicating enhanced emersion tolerance. When we compared the heat failure rate (closely linked to z, Equation (2)) for emersed oysters ($eA = 1.782\ eV$), these parameter values were similar to those for emersed tropical oysters *Crassostrea rhizophorae* ($eA = 1.979\ eV$). This indicates such low emersed heat failure rates (and therefore high values of z) may be a common response in intertidal oysters (Littlewood, 1989). Heat failure in immersed oysters ($eA = 3.283\ eV$) is much more rapid than non-lethal traits in permissive temperature ranges such as growth and movement speed (0.5-0.8 eV), aligning with expectations that temperature increases in extreme, non-permissive temperature ranges will have an exponential effect on organism persistence and result in lethal effects (Jørgensen et al., 2022). While emersed oysters had a much lower activation energy than immersed oysters, indicating a degree of aerial warming will have a smaller proportional effect on heat failure, our calculated value is still much higher than expected for traits found in non-lethal traits. Importantly, *C. virginica* lives much closer to its thermal limits when emersed than immersed (Deutsch et al., 2008; Somero, 2002; Somero, 2010), so this lower heat failure rate may not provide much buffer in an already extreme, and warming, environment.

Thermal death time curves themselves are emergent statistical phenomena of many mechanisms working together on different scales of time and biological organization, with a baseline pattern explained by the physics of temperature. The intersecting, and therefore divergent, response of survival time to temperature across exposure treatments is likely due to interactions of multiple adaptive physiological traits and behavior rather than a tradeoff in a single phenotype (Fig. 6). Two potential mechanisms may be responsible for this observed effect: evaporative cooling through gaping and metabolic depression. Gaping behavior can cool bivalves compared to ambient temperatures and concurrently improve oxygenation through enhanced gas exchange across wet gill tissue (Hicks and McMahon, 2003; Nicastro et al., 2012; Nicholson, 2002). Numerical heat budget models suggest evaporation of water from wet tissues during gaping can cool overall bivalve body temperatures by several degrees, dependent on ambient humidity, wind speed, and solar radiation (Helmuth, 1998). However, evidence suggests this may not have an appreciable effect in the field (Jost and Helmuth, 2007; Nicastro et al., 2012). The rates of evaporation in the experimental incubators were limited by the constant levels of humidity ($\sim$75%) across treatments, thus controlling for one of these covariates. We observed, but did not measure, periodic gaping within the first few hours of incubator experiments that could potentially lower oyster body temperature compared to the ambient chamber temperature. At lower durations and higher temperatures, emersed oysters

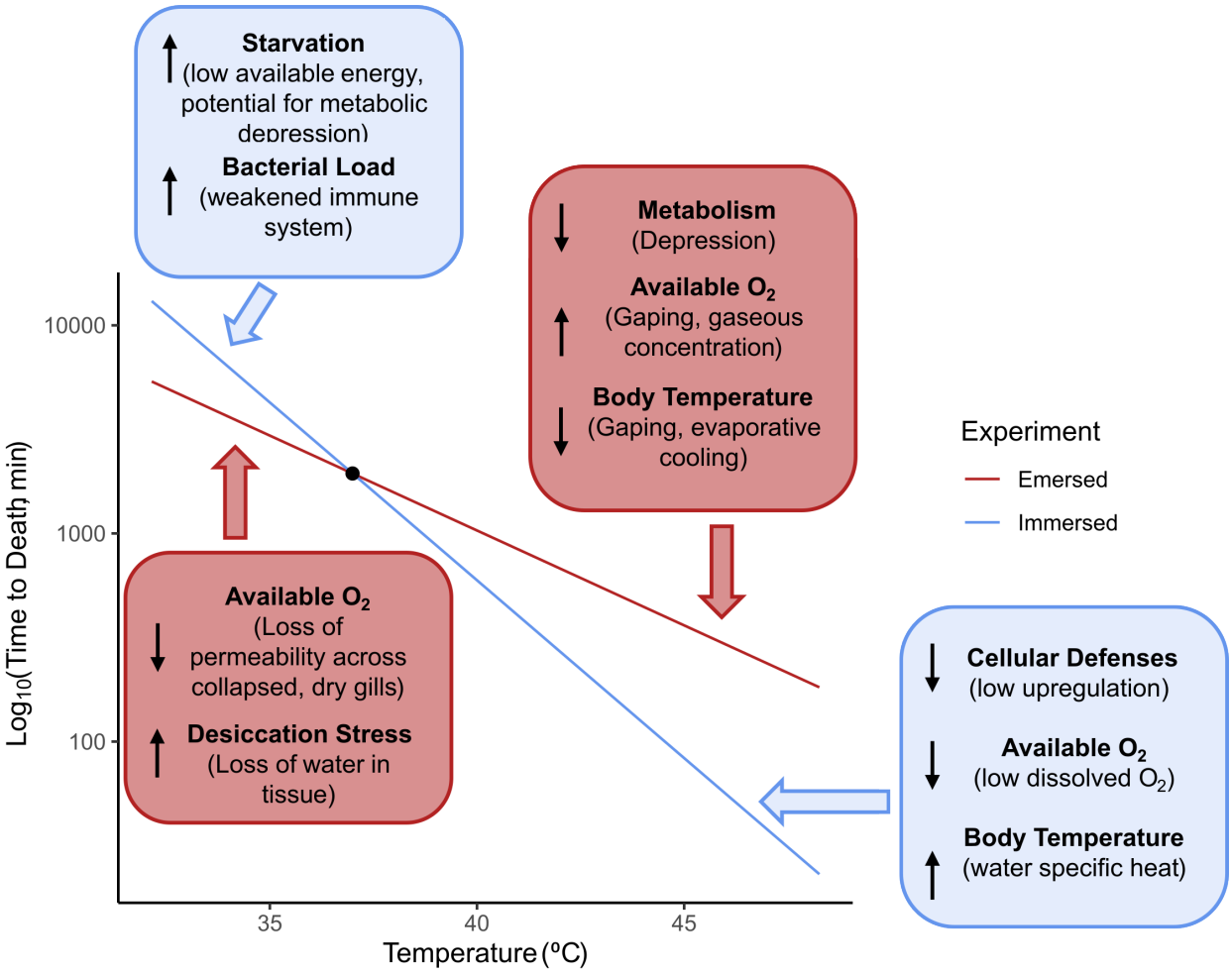

Figure 6: Conceptual diagram of the proposed physiological, physical, and behavioral drivers of immersed and emersed TDT curves. At lower lethal temperatures, immersed oysters (blue) may die due to starvation and increased susceptibility to bacterial infection, increasing demands on energy for basic maintenance. Emersed oysters (red) experience desiccation stress over long periods of time, impacting their ability to exchange gases across tissues and perform other organ functions. Over higher lethal temperatures, immersed oysters may die due to an insufficient supply of dissolved oxygen, inability to behaviorally thermoregulate via gaping, and lack of an environmental signal to induce cellular defenses. Finally, emersed oysters may depress their metabolism and upregulate cellular defenses in response to an emersion environmental signal, thereby extending their time to death compared to immersed counterparts. They additionally may gape, which can increase oxygen availability for aerobic metabolism as well as cooling the individual through evaporation. Not shown are molecular processes such as protein denaturation and loss of membrane layer integrity.

may survive longer due to their higher partial pressure of oxygen in air across still-moist tissues compared to warmed seawater. Conversely, over lower temperatures on the TDT curve (below TDT curve inflection at 37 °C), oysters were subjected to longer periods of air exposure which can lead to drastic losses in tissue weight due to desiccation, potentially leading to a loss of resistance time (Helmuth, 1998; Lent, 1968; Nicastro et al., 2012; Overton et al., 2024). Given gas exchange occurs in wet mantle and gill tissue, the loss of resistance time in emersed oysters may also be due to a prolonged period of anaerobic metabolism compared to an equivalent exposure duration in immersed oysters.

Oxygen limitation likely plays a critical role in the differentiation between immersed and emersed TDT curves. Aerobic metabolism often cannot meet the energetic demands of survival under extreme stress, which can further be exacerbated by a reduction of dissolved oxygen in warm water (Sokolova, 2013; Sokolova et al., 2012). In these cases, an organism may use anaerobic metabolism to attempt to keep with energy demands in the short term at the expense of long-term fitness. Heart rate correlates with oxygen uptake in bivalves, with heart rate increasing in tandem with temperature as bivalves attempt to maintain their aerobic scope through increased oxygen uptake (pejus), though this is often offset with some amount of anaerobiosis (Eymann et al., 2020; Götze et al., 2025). Once aerobic metabolism fails, and energy is produced almost exclusively through anaerobic pathways (pessimum), arrhythmia and bradycardia occur (Liao et al., 2021). Thus, slowing cardiac rate and arrhythmia in oysters should occur either once oxygen capacity is not met and a switch from aerobiosis to anaerobiosis occurs, and cessation of cardiac activity should occur when anaerobic metabolism can no longer meet energy demands through metabolic means (Eymann et al., 2020; Pörtner et al., 2017). The tight connection between cardiac activity, loss of energetic currency, and death argues in favor of monitoring organ function with biosensors to determine time to death in non-model species, rather than visual assays (e.g. knock-down).

In our experiments, immersed oysters did not have any supplemental oxygen or air bubbled into their tanks other than the "fresh" preheated seawater. Thus, the oxygen availability in the tank treatments likely decreased with an increasing assay temperature. Further, as oysters respired, boundary layers of deoxygenated water likely formed around each oyster, further reducing available dissolved oxygen (Verberk and Atkinson, 2013; Verberk et al., 2016). Over short intervals, oysters can override such dissolved oxygen limitations in water by metabolizing anaerobically, but without supplemental oxygen oysters in general can only survive in non-steady state metabolism for short periods. Emersed oysters may have been able to exploit the higher concentration of atmospheric oxygen to avoid anaerobiosis in the short term through gaping, especially if desiccation stress is low (McMahon, 1988). Alternatively, emersed oysters may enter metabolic depression as an anticipatory action to long-term emersion stress, thereby reducing their oxygen demands for aerobic metabolism and enabling longer survival at particularly stressful high air temperatures (Bjelde and Todgham, 2013; Guppy and Withers, 1999; Hui et al., 2022; Marshall and McQuaid, 1991; Marshall and McQuaid, 2010; Shick et al., 1988). Metabolic depression is further enabled by the cessation of non-basal maintenance behaviors such as feeding (McMahon, 1988). Metabolic strategies can

differ between mollusk species, however; *Lottia* limpets displayed metabolic depression in stressful submersion and emersion temperatures, but emersed limpets had a higher final cardiac breakpoint temperature (Bjelde and Todgham, 2013), while *Mytilus* mussels experienced bradycardia when exposed to air (Shick et al., 1988). Critically, the oysters we used in laboratory experiments were acclimated to normoxic submerged conditions only, which may have limited their ability to deploy metabolic depression during emersed experiments and potentially provide an overly conservative estimation of oyster time to death in intertidally-acclimated populations (Altieri, 2006; Meng et al., 2018; Shick et al., 1988; Zwaan and Eertman, 1996).

4.2 Dynamic Tolerance Models Using TTL-Switching Outperform Emersed and Immersed Thermal Tolerance Models

For the first time, we modeled survival in the intertidal zone using an adjusted dynamic survival model to account for different thermal tolerance strategies over time in a single organism. Since the TDT curves of each exposure type intersect, oysters best tolerate immersion below 37 °C and emersion above 37 °C. Considering low tide temperatures exceeded 40 °C in the field, while water temperature rarely exceeded 30 °C (values above this occur occasionally as loggers cooled down immediately following immersion), mortality mainly occurred in response to low tide-conditions. Emersion temperature is likely an adaptive filter, where selective pressure to evolve behavior and mechanisms that can cope with extreme air temperatures may be operating in these oyster populations (Dong, 2023; Leeuwis and Gamperl, 2022). However, since different mechanisms (both physiological and behavioral) appear to operate in composite on different ends of each TDT curve, the overall thermal tolerance observed may be a product of multiple mechanisms rather than a single adaptive or tradeoff strategy (Jørgensen et al., 2019). This also suggests that mechanisms of stress accumulation and recovery differ not only between acute and chronic temperatures, but also exposure type. The extent to which recovery between emersion events occurs will depend on the immersed water temperature, indicating a thermal load sensitivity for intertidal organisms will need to account for differential recovery across tidal emergence states (Arnold et al., 2025; Buckley et al., 2025; Ma et al., 2018; Seuront et al., 2019).

4.3 Experimentally Derived TTLs overpredict Field Survival

Our standard intertidal dynamic tolerance model generally overpredicted field mortality across our two field sites in Great Bay (RMSE = 6.4 and 3.33, Brackett's Point and JEL). A potential confounding issue of using our lab-derived TTLs within the intertidal dynamic survival model was the difference in acclimation regime for the laboratory oysters and the field oysters. Oysters used in lab experiments were kept in constant submersion conditions in water a few degrees cooler than the temperature of Great Bay during field oyster deployment, and field oysters were able to acclimate to permissive intertidal conditions before more extreme low tide conditions occurred later in the summer. Plasticity arising from acclimation and heat hardening to constant conditions in laboratory settings are known to induce plastic responses in ectotherms, although the effect size and

direction of acclimation can vary across populations, species, and experimental methods (Barley et al., 2021; Calosi et al., 2016; Oliver and Palumbi, 2011; Schaum et al., 2022; van Heerwaarden and Kellermann, 2020; Villeneuve et al., 2021). Prior exposure to variable temperatures, such as those that occur in the intertidal, can either enhance performance or become deleterious depending on the frequency and amplitude of variation against background temperature (Pereira et al., 2025; Seuront et al., 2019; Vajedsamiei et al., 2021; Walton et al., 2025). Our simulation calibration indicates that modest increases in intercept or slope (increased $CT_{max(1min)}$ or decreased z) of the underlying emersed TDT curve better predicted field data at our two study sites (RMSE = 0.93 and 2.29, Brackett's Point and JEL). While we cannot definitively attribute these calibrated parameters to warmer or more variable acclimation, the shift in curve parameters are consistent with experiments explicitly testing the effects of sublethal acclimation on TDT curves in *Drosophila* flies (Baeza Icaza et al., 2025) and the Pacific oyster *Magallana gigas* (Rajagopal et al., 2005). It is further possible that the immersed TDT curve also shifts due to intertidal acclimation. However, because mortality accumulation was extremely low to nonexistent when oysters were submerged, our calibration approach did not identify more optimal TDT parameters.

We observed a 55% drop in survival at JEL over a period of two weeks that was not explainable by temperature alone. We hypothesize that there was some environmental event or plastic response that caused oysters to be more susceptible to heat stress. Hyposaline events are a well-known contributor to oyster mortality, particularly when occurring in tandem with elevated temperatures (Bible et al., 2017; Cheng et al., 2017; Du et al., 2021; Goff et al., 2016). However, salinity in Great Bay as measured from a nearby NERRS buoy never dropped below a normally tolerable 20 PSU during the study period. Hypoxia, another potential contributing factor to oyster mortality (Davis et al., 2023), did not occur in Great Bay in the summer of 2025 - dissolved oxygen values in the early summer never went below 6 mg/L (station GRBGBWQ, NERRS CDMO).

If environmental conditions did not directly cause additional mortality, then biological causes may be responsible. In Great Bay, oysters spawning starts in May as indicated by the presence of D-hinge larvae in the water column by early June (Stasse et al., 2022). Reproductive investment for gametogenesis and spawning early in the season may exhaust energy reserves, resulting in higher demands on metabolism to supply energy under extreme temperature conditions (Li et al., 2007; Wendling and Wegner, 2013). Time to death could therefore have been faster than expected because our field oysters spawned, lowering their resistance to thermal challenge. Finally, bacterial infection and disease could have weakened oysters at JEL, but not at Brackett's Point. *Vibrio* infections are more prevalent in *C. virginica* in warmer waters, as these conditions are more conducive to bacterial growth (Cowan et al., 2023; Green et al., 2019; Perdue et al., 1981; Siboni et al., 2024; Wendling and Wegner, 2013). However, water temperatures during the anomalous mortality event were cooler than later in the summer - only air temperatures had large June anomalies. Anoxic environments provide an advantage to anerobioic bacteria, particularly in warm water, which can also produce harmful hydrogen sulfide (H_2S; (Steeves et al., 2025)). It is possible that immersed oysters in our laboratory experiments were limited by bacterial growth, particularly over long temperature

exposures. Further, recently spawned oysters have weaker immune system responses, which can provide opportunities for infection at otherwise non lethal temperatures (Li et al., 2007). Different oyster mortality events may be caused by different factors at different times of the year, with temperature only one of many stressors acting on intertidal populations. Our modeling framework allows us to set a null expectation for mortality due to temperature alone, allowing future work to identify when other factors are likely at play.

4.4 Impact of Future Warming

Our warming simulations indicate that aerial heatwaves are likely to be more deleterious to intertidal oysters than marine heatwaves in isolation. We calculated 9.5% greater mortality when only air temperature is increased compared to only water temperature for the oysters acclimated at Brackett's Point. Many intertidal thermal tolerance assays focus on submerged thermal tolerance only, which may not be informative if the warming tolerance of fully submerged organisms is much higher than those experienced during emersion (Deutsch et al., 2008; Vajedsamiei et al., 2024; Walton et al., 2025). For example, the widespread mass mortality events of intertidal bivalves during the 2021 Pacific Northwest heatdome were mostly correlated with repeated low tide exposure of intertidal areas during daily solar maxima (Hesketh and Harley, 2023; Raymond et al., 2022; Raymond et al., 2024). Warming of water temperature in temperate marine environments is likely important, but in the context of recovery rather than outright contributing to the accumulation of thermal stress (Arnold et al., 2025; Buckley et al., 2025; Ørsted et al., 2025; Seuront et al., 2019). Future work can identify the point at which submersion ceases to aid in recovery, and instead antagonistic stress accumulation processes take over - our model can then be improved to integrate potential temperature-dependent recovery.

It is also possible that oysters will adapt to future warming conditions, although such genetic shifts in a population will be dependent on the strength of selective pressure and genetic variation within intertidal oyster populations (Andreassen et al., 2025; Morgan et al., 2020). One meta-analysis identifies 80.5% of variation in acute tolerance (TDT curve intercept, $CT_{max(1min)}$) arises from genetic rather than plastic components, and that plasticity overall is limited in ability to dramatically shift TDT curves (Molina et al., 2024). It is worth remembering that atmospheric heatwaves extreme enough to result in mortality are already occurring globally, and that a 2 °C increase in air temperature may be an underestimate of intertidal body temperatures during the most extreme atmospheric heatwaves.

4.5 Limitations and Future Directions

We made a number of assumptions when building our mortality prediction framework for intertidal oysters in order to make such an analysis tractable. Oysters used in the thermal tolerance experiments and the field deployments all originated from hatchery stock, rather than wild oysters adapted to local intertidal thermal regimes. These oysters may have acclimated to local conditions during the year they were immersed at an aquaculture farm, but were not exposed to an intertidal

regime before experimentation. Subtidal populations of the Pacific oyster *C. gigas* exhibits faster onset of anaerobiosis and metabolic depression when emersed compared to intertidal populations, which may have an adaptive genetic basis (Meng et al., 2018). We would therefore expect our base intertidal dynamic model to overestimate mortality for wild, intertidal oysters in the absence of other stressors. Parameterizing dynamic tolerance models directly from field mortality data using Bayesian approximation techniques is likely to result in enhanced prediction accuracy (Vajedsamiei et al., 2024). Even so, the shape of underlying TDT curves and survival functions for oysters across exposure likely change with acclimation, energetic state, and age within a single summer, precluding even our enhanced intertidal model from performing equally well across the target data window. Finally, assumptions of consistent variance in $S(t)$ across temperatures within the intertidal dynamic tolerance model may not be appropriate (Bullard et al., 2026).

We assumed oysters would recover from heat stress during each intertidal cycle immediately upon immersing upon the next cycle. Multiple extreme aerial exposures are known to weaken intertidal invertebrates, indicating that while some recovery does occur during submersion in cooler water, recovery is not perfect. Multiple exposures of the blue mussel *Mytilus edulis* to air temperatures up to 41 °C following for five days resulted in a steadily decreasing survival rate on each subsequent day, indicating resistance declined even with realistic immersion durations in ambient seawater (Seuront et al., 2019). This indicates that heat hardening and plasticity does not occur, and that such exposures likely overextend mussels' ability to deploy molecular and cellular protection to heat challenge (Clarke et al., 2000). The extent to which recovery can occur is further set by ambient seawater conditions - warmer water forces the limpet *Patella vulgata* to increase its basal metabolic rate, impairing their ability to repair during immersion (Seabra et al., 2016). This indicates that higher seawater temperature during immersion may play an equal role in mortality probability as emersion temperature, even in temperate systems like Great Bay. Our model could be further improved by setting a seawater temperature threshold beyond which only partial recovery can occur, which itself is likely a continuous function dependent on time lag from emersion, seawater temperature, and immersion duration. Future experimentation and alteration of the intertidal dynamic tolerance model should be undertaken to parameterize a more realistic recovery process.

5 Conclusion

The global increase in heatwave events and corresponding marine invertebrate mass mortality events challenges our ability to produce quantitative predictions of population impacts. We demonstrated an experimental and modelling approach that quantifies thermal stress accumulation in the oyster *C. virginica* in a dynamic and fluctuating intertidal environment. While our laboratory-parameterized model overpredicted field mortality, we were able to generate more accurate predictions once we optimized parameters for a more variable acclimation regime. While explicitly our framework addresses intertidal systems, the advances we made to understand and pre-

dict intertidal mortality can directly help address some of the pressing problems of understanding unprecedented environmental and biological fluctuations by incorporating changing physiological states (i.e. immersed v. emersed thermal tolerance) into mechanistic predictions. The autocorrelation of multiple events means predictions must be able to account for both recovery and time-dependent stress accumulation in a marine system (Denny et al., 2009; Gerhard et al., 2023). Thus, intertidal environments pose a tractable, predictable system for observing the impacts of multiple exposures on organism mortality.

6 List of symbols and Abbreviations

CML – Coastal Marine Station (University of New Hampshire) IR - Infrared JEL – Jackson Estuarine Lab (University of New Hampshire) OCLTT – Oxygen- and capacity-limited thermal tolerance TDT – Thermal Death Time TLS – Thermal Load Sensitivity TTL – Thermal Tolerance Landscape

7 Acknowledgments

Franny Lux, Nate Rennells, Jessica Robinson, Dave Shay, and Grant McKown provided critical logistical and facilities support assistance at UNH's Jackson Estuarine Lab and Coastal Marine Lab. We thank Josie DeMerit, Tianyi Duan, and Ella Williams for their assistance during lab and field work. Special thanks to Selina Cheng, Michaela Edwards, and Jannine Chamorro for assisting with field deployments and brainstorming.

8 Competing interests

The authors declare no competing interests.

9 Author contributions

Conceptualization — A.R.V., B.J., E.R.W.; Data curation — A.R.V.; Formal Analysis — A.R.V.; Funding acquisition — A.R.V., B.J., E.R.W., Investigation — A.R.V.; Methodology — A.R.V., B.J., E.R.W., Resources — B.J.; Software — A.R.V.; Supervision — B.J., E.R.W.; Visualization — A.R.V.; Writing – original draft — A.R.V.; Writing – review and editing — A.R.V., B.J., E.R.W.

10 Funding

Partial funding was provided by the New Hampshire Agricultural Experiment Station. This work (scientific contribution number X,XXX) was supported by the Hatch program (NH 00718-C

and NH 00714-R), project award numbers (7004018 and 7005066), from the US Department of Agriculture's National Institute of Food and Agriculture and the state of New Hampshire. Additional funding to ARV was provided by the New Hampshire Sea Grant Graduate Research Fellowship, the University of New Hampshire School of Marine Science and Ocean Engineering Graduate Research Fund, and the University of New Hampshire Graduate School Dissertation Year Fellowship.

11 Data availability

Code and data used in the production of this manuscript are available at the anonymized repository https://anonymous.4open.science/r/oyster$_TDT_manuscript2026-5F07$. Code and data will be uploaded to Zenodo and Data Dryad upon acceptance for publication.

12 References

References

Abbas, A., Collins, M., Ellis, R., Spicer, J. I. and Truebano, M. (2024). Heat hardening improves thermal tolerance in abalone, without the trade-offs associated with chronic heat exposure. *Journal of Thermal Biology* 103963.

Alruiz, J. M., Peralta-Maraver, I., Bozinovic, F., Santos, M. and Rezende, E. L. (2022). Thermal tolerance in Drosophila: Repercussions for distribution, community coexistence and responses to climate change. *J. Anim. Ecol.* **91**, 655–667.

Altieri, A. H. (2006). Inducible variation in hypoxia tolerance across the intertidal–subtidal distribution of the blue mussel Mytilus edulis. *Mar Ecol Prog Ser* **325**, 295–300.

Andreassen, A. H., Clements, J. C., Morgan, R., Spatafora, D., Metz, M., Åsheim, E. R., Pélabon, C. and Jutfelt, F. (2025). Evolution of warming tolerance alters physiology and life history traits in zebrafish. *Nat. Clim. Chang.* **15**, 665–672.

Angilletta, M. J. (2009). *Thermal adaptation: a theoretical and empirical synthesis*. New York, NY: Oxford University Press.

Arnold, P. A., Noble, D. W. A., Nicotra, A. B., Kearney, M. R., Rezende, E. L., Andrew, S. C., Briceño, V. F., Buckley, L. B., Christian, K. A., Clusella-Trullas, S., et al. (2025). A framework for modelling thermal load sensitivity across life. *Glob Chang Biol* **31**,.

Arnoldi, J.-F., Jackson, A. L., Peralta-Maraver, I. and Payne, N. L. (2025). A universal thermal performance curve arises in biology and ecology. *Proc. Natl. Acad. Sci.* **122**, e2513099122.

Baeza Icaza, A., Poblete Ahumada, G., Rezende, E. L. and Peralta-Maraver, I. (2025). Warm acclimation reduces the sensitivity of Drosophila species to heat stress at ecologically relevant scales. *J. Anim. Ecol.* **94**,.

Bailey, L. D. and van de Pol, M. (2016). Tackling extremes: challenges for ecological and evolutionary research on extreme climatic events. *J. Anim. Ecol.* **85**, 85–96.

Bakhmet, I., Abessa, D., Buruaem, L. and Bonnail, E. (2015). A Non-Invasive Technique for Recording the Cardiac Activity of the Tropical-Subtropical Mangrove Oyster Crassostrea brasiliana. *Pan-American Journal of Aquatic Sciences* **10**, 249–253.

Barley, J. M., Cheng, B. S., Sasaki, M., Gignoux-Wolfsohn, S., Hays, C. G., Putnam, A. B., Sheth, S., Villeneuve, A. R. and Kelly, M. (2021). Limited plasticity in thermally tolerant ectotherm populations: evidence for a trade-off. *Proc. R. Soc. B.* **288**, 20210765.

Bates, D., Mächler, M., Bolker, B. and Walker, S. (2015). Fitting Linear Mixed-Effects Models Using lme4. *J Stat Softw* **67**, 1–48.

Bates, A. E., Helmuth, B., Burrows, M. T., Duncan, M. I., Garrabou, J., Guy-Haim, T., Lima, F., Queiros, A. M., Seabra, R., Marsh, R., et al. (2018). Biologists ignore ocean weather at their peril. *Nature* **560**, 299–301.

Bible, J. M., Cheng, B. S., Chang, A. L., Ferner, M. C., Wasson, K., Zabin, C. J., Latta, M., Sanford, E., Deck, A. and Grosholz, E. D. (2017). Timing of stressors alters interactive effects on a coastal foundation species. *Ecology* **98**, 2468–2478.

Bjelde, B. E. and Todgham, A. E. (2013). Thermal physiology of the fingered limpet Lottia digitalis under emersion and immersion. *Journal of Experimental Biology* **216**, 2858–2869.

Briscoe, N. J., Morris, S. D., Mathewson, P. D., Buckley, L. B., Jusup, M., Levy, O., Maclean, I. M. D., Pincebourde, S., Riddell, E. A., Roberts, J. A., et al. (2023). Mechanistic forecasts of species responses to climate change: The promise of biophysical ecology. *Glob Chang Biol* **29**, 1451–1470.

Brown, J. H., Gillooly, J. F., Allen, A. P., Savage, V. M. and West, G. B. (2004). Toward a metabolic theory of ecology. *Ecology* **85**, 1771–1789.

Buckley, L. B., Huey, R. B. and Ma, C.-S. (2025). How damage, recovery, and repair alter the fitness impacts of thermal stress. *Integr Comp Biol* **65**, 1061–1075.

Bullard, G. W., Buckley, L. B. and Kingsolver, J. G. (2026). Moving beyond mean thermal death times to assess organismal responses to stressful temperatures.

Burnett, N. P., Seabra, R., de Pirro, M., Wethey, D. S., Woodin, S. A., Helmuth, B., Zippay, M. L., Sarà, G., Monaco, C. and Lima, F. P. (2013). An improved noninvasive method for measuring heartbeat of intertidal animals. *Limnol. Oceanogr. Methods* **11**, 91–100.

Burnham, K. P. and Anderson, D. R. eds. (2002). *Model selection and multimodel inference*. New York, NY: Springer New York.

Calosi, P., Wit, P. D., Thor, P. and Dupont, S. (2016). Will life find a way? Evolution of marine species under global change. *Evol Appl* **9**, 1035–1042.

Castañeda, L. E., Rezende, E. L. and Santos, M. (2015). Heat tolerance in Drosophila subobscura along a latitudinal gradient: Contrasting patterns between plastic and genetic responses. *Evolution* **69**, 2721–2734.

Cheng, B. S., Komoroske, L. M. and Grosholz, E. D. (2017). Trophic sensitivity of invasive predator and native prey interactions: integrating environmental context and climate change. *Funct Ecol* **31**, 642–652.

Clarke, A., Mill, P. J. and Grahame, J. (2000). The nature of heat coma in Littorina littorea (Mollusca: Gastropoda). *Marine Biology* **137**, 447–451.

Cowan, M. W., Pearce, C. M., Finston, T., Meyer, G. R., Marshall, R., Evans, W., Sutherland, T. F. and de la Bastide, P. Y. (2023). Role of the *Vibrio* community, reproductive effort, and environmental parameters in intertidal Pacific oyster summer mortality in British Columbia, Canada. *Aquaculture* **565**, 739094.

Davis, A. M., Plough, L. V. and Paynter, K. T. (2023). Intraspecific patterns of mortality and cardiac response to hypoxia in the eastern oyster, *Crassostrea virginica*. *Journal of Experimental Marine Biology and Ecology* **566**, 151921.

de Carvalho, I. S. C., Cantanhêde, S. M., Hamoy, M., da Cruz Freitas Júnior, J. R. and Amado, L. L. (2022). Cardiac responses in *Crassostrea gasar*: An experimental approach of how the tidal cycle influences the heart function of the mangrove oyster. *Comparative Biochemistry and Physiology Part A: Molecular & Integrative Physiology* **271**, 111264.

Dell, A. I., Pawar, S. and Savage, V. M. (2011). Systematic variation in the temperature dependence of physiological and ecological traits. *Proc. Natl. Acad. Sci.* **108**, 10591–10596.

Denny, M. W. (2017). The fallacy of the average: on the ubiquity, utility and continuing novelty of Jensen's inequality. *Journal of Experimental Biology* **220**, 139–146.

Denny, M. W., Hunt, L. J. H., Miller, L. P. and Harley, C. D. G. (2009). On the prediction of extreme ecological events. *Ecological Monographs* **79**, 397–421.

Deschamps, M., Giménez, L., Astley, C., Boersma, M. and Torres, G. (2025). Heatwave duration, intensity and timing as drivers of performance in larvae of a marine invertebrate. *Sci Rep* **15**, 15949.

Deutsch, C. A., Tewksbury, J. J., Huey, R. B., Sheldon, K. S., Ghalambor, C. K., Haak, D. C. and Martin, P. R. (2008). Impacts of climate warming on terrestrial ectotherms across latitude. *Proceedings of the National Academy of Sciences, USA* **105**, 6668–6672.

Dong, Y.-W. (2023). Roles of multi-level temperature-adaptive responses and microhabitat variation in establishing distributions of intertidal species. *Journal of Experimental Biology* **226**, jeb245745.

Dowd, W. W. and Denny, M. W. (2020). A series of unfortunate events: characterizing the contingent nature of physiological extremes using long-term environmental records. *Proceedings: Biological Sciences* **287**, 1–9.

Dowd, W. W., King, F. A. and Denny, M. W. (2015). Thermal variation, thermal extremes and the physiological performance of individuals. *Journal of Experimental Biology* **218**, 1956–1967.

Du, J., Park, K., Jensen, C., Dellapenna, T. M., Zhang, W. G. and Shi, Y. (2021). Massive oyster kill in Galveston Bay caused by prolonged low-salinity exposure after Hurricane Harvey. *Science of The Total Environment* **774**, 145132.

Dwane, C., Rundle, S. D., Tills, O., Rezende, E. L., Galindo, J., Rolán-Alvarez, E. and Truebano, M. (2021). Divergence in Thermal Physiology Could Contribute to Vertical Segregation in Intertidal Ecotypes of Littorina saxatilis. *Physiol Biochem Zool* **94**, 353–365.

Dwane, C., Komoroske, L. M., Rugila, A. L., Bentley, B. P., Rawson, E., Clark, E., Nichols, G., Newbrey, M., Bucari, E., Yan, C., et al. (2025). Adaptation to warm environments with a fast pace of life in a marine predatory snail.

Ern, R., Andreassen, A. H. and Jutfelt, F. (2023). Physiological mechanisms of acute upper thermal tolerance in fish. *Physiology* **38**, 141–158.

Eymann, C., Götze, S., Bock, C., Guderley, H., Knoll, A. H., Lannig, G., Sokolova, I. M., Aberhan, M. and Pörtner, H.-O. (2020). Thermal performance of the European flat oyster, Ostrea edulis (Linnaeus, 1758)—explaining ecological findings under climate change. *Mar Biol* **167**, 17.

Federighi, H. (1929). Temperature characteristics for the frequency of heart beat in Ostrea virginica Gmelin. *J. Exp. Zool.* **54**, 89–94.

Feng, S. Y. (1965). Heart rate and lecuocyte circulation in *Crassostrea virginica* (Gmelin). *The Biological Bulletin* **128**, 198–210.

Feng, S. Y. and Van Winkle, W. (1975). The effect of temperature and salinity on the heart beat of *Crassostrea virginica*. *Comparative Biochemistry and Physiology Part A: Physiology* **50**, 473–476.

Gerhard, M., Koussoroplis, A.-M., Raatz, M., Pansch, C., Fey, S. B., Vajedsamiei, J., Calderó-Pascual, M., Cunillera-Montcusí, D., Juvigny-Khenafou, N. P. D., Polazzo, F., et al. (2023). Environmental variability in aquatic ecosystems: Avenues for future multifactorial experiments. *Limnol Oceanogr Lett* **8**, 247–266.

Gilman, S. E., Harley, C. D. G., Strickland, D. C., Vanderstraeten, O., O'Donnell, M. J. and Helmuth, B. (2006). Evaluation of effective shore level as a method of characterizing intertidal wave exposure regimes. *Limnology & Ocean Methods* **4**, 448–457.

Giménez, L. (2023). A geometric approach to understanding biological responses to environmental fluctuations from the perspective of marine organisms. *Mar. Ecol. Prog. Ser.* **721**, 17–38.

Goff, J. A., Lugrin, L., Gulick, S. P., Thirumalai, K. and Okumura, Y. (2016). Oyster reef die-offs in stratigraphic record of Corpus Christi Bay, Texas, possibly caused by drought-driven extreme salinity changes. *Holocene* **26**, 511–519.

Götze, S., Reddin, C. J., Ketelsen, I., Busack, M., Lannig, G., Bock, C. and Pörtner, H.-O. (2025). Cardiac performance mirrors the passive thermal tolerance range in the oyster *Ostrea edulis*. *J. Exp. Biol.* **228**, JEB249750.

Green, T. J., Siboni, N., King, W. L., Labbate, M., Seymour, J. R. and Raftos, D. (2019). Simulated marine heat wave alters abundance and structure of vibrio populations associated with the pacific oyster resulting in a mass mortality event. *Microb Ecol* **77**, 736–747.

Guppy, M. and Withers, P. (1999). Metabolic depression in animals: physiological perspectives and biochemical generalizations. *Biol. Rev.* **74**, 1–40.

Harley, C. D. G. and Helmuth, B. S. T. (2003). Local- and regional-scale effects of wave exposure, thermal stress, and absolute versus effective shore level on patterns of intertidal zonation. *Limnology & Oceanography* **48**, 1498–1508.

Harris, R. M. B., Beaumont, L. J., Vance, T. R., Tozer, C. R., Remenyi, T. A., Perkins-Kirkpatrick, S. E., Mitchell, P. J., Nicotra, A. B., McGregor, S., Andrew, N. R., et al. (2018). Biological responses to the press and pulse of climate trends and extreme events. *Nature Clim Change* **8**, 579–587.

Helmuth, B. S. (1998). Intertidal mussel microclimates: Predicting the body temperature of a sessile invertebrate. *Ecol Monogr* **68**, 51–74.

Hesketh, A. V. and Harley, C. D. G. (2023). Extreme heatwave drives topography-dependent patterns of mortality in a bed-forming intertidal barnacle, with implications for associated community structure. *Glob Chang Biol* **29**, 165–178.

Hicks, D. W. and McMahon, R. F. (2003). Temperature and relative humidity effects on water loss and emersion tolerance of Perna perna (L.)(Bivalvia: Mytilidae) from the Gulf of Mexico. *Bull. Mar. Sci.* **72**, 135–150.

Hobday, A. J., Oliver, E., Sen Gupta, A., Benthuysen, J., Burrows, M., Donat, M., Holbrook, N., Moore, P., Thomsen, M., Wernberg, T., et al. (2018). Categorizing and naming marine heatwaves. *Oceanog* **31**, 162–173.

Hui, T. Y., Crickenberger, S., Lau, J. W. T. and Williams, G. A. (2022). Why are 'suboptimal' temperatures preferred in a tropical intertidal ectotherm? *J. Anim. Ecol.* **91**, 1400–1415.

Jørgensen, L. B., Malte, H. and Overgaard, J. (2019). How to assess Drosophila heat tolerance: Unifying static and dynamic tolerance assays to predict heat distribution limits. *Funct Ecol* **33**, 629–642.

Jørgensen, L. B., Malte, H., Ørsted, M., Klahn, N. A. and Overgaard, J. (2021). A unifying model to estimate thermal tolerance limits in ectotherms across static, dynamic and fluctuating exposures to thermal stress. *Sci Rep* **11**, 12840.

Jørgensen, L. B., Ørsted, M., Malte, H., Wang, T. and Overgaard, J. (2022). Extreme escalation of heat failure rates in ectotherms with global warming. *Nature* **611**, 93–98.

Jost, J. and Helmuth, B. (2007). Morphological and Ecological Determinants of Body Temperature of Geukensia demissa, the Atlantic Ribbed Mussel, and Their Effects On Mussel Mortality. *Biol Bull* **213**, 141–151.

Koehring, V. (1937). The rate of heart beat in clams. *Bulletin of the Mount Desert Island Biological Laboratory* **Thirty-ninth season**, 25–26.

Leeuwis, R. H. J. and Gamperl, A. K. (2022). Adaptations and plastic phenotypic responses of marine animals to the environmental challenges of the high intertidal zone. In *Oceanography and marine biology*, p. CRC Press.

Lent, C. M. (1968). Air-gaping by the Ribbed mussel, Modiolus demissus (Dillwyn): Effects and adaptive significance. *The Biological Bulletin* **134**, 60–73.

Lenth, R. V., Piaskowski, J., Banfai, B., Bolker, B., Buerkner, P., Giné-Vázquez, I., Hervé, M., Jung, M., Love, J., Miguez, F., et al. (2025). Emmeans: Estimated Marginal Means, aka Least-Squares Means.

Levinton, J. S., Volkenborn, N., Gurr, S., Correal, K., Villacres, S., Seabra, R. and Lima, F. P. (2020). Temperature-related heart rate in water and air and a comparison to other temperature-related measures of performance in the fiddler crab *Leptuca pugilator* (Bosc 1802). *Journal of Thermal Biology* **88**, 102502.

Li, Y., Qin, J. G., Abbott, C. A., Li, X. and Benkendorff, K. (2007). Synergistic impacts of heat shock and spawning on the physiology and immune health of *Crassostrea gigas* : an explanation for summer mortality in Pacific oysters. *American Journal of Physiology-Regulatory, Integrative and Comparative Physiology* **293**, R2353–R2362.

Liao, M., Li, G., Wang, J., Marshall, D. J., Hui, T. Y., Ma, S., Zhang, Y., Helmuth, B. and Dong, Y. (2021). Physiological determinants of biogeography: The importance of metabolic depression to heat tolerance. *Glob Chang Biol* **27**, 2561–2579.

Ligges, U. ., Short, T., Kienzle, P., Schnackenberg, S., Billinghurst, D., Borchers, H.-W., Carezia, A., Dupuis, P., Eaton, J. W., Farhi, E., et al. (2024). Signal: Signal Processing.

Lima, F. P., Pereira, L., Loureiro, B., Humet, M. and Seabra, R. (2025). A fully automated heart frequency logger for shelled invertebrates and associated data processing R package. *Methods Ecol Evol* **16**, 2797–2806.

Littlewood, D. T. J. (1989). Thermal tolerance and the effects of temperature on air-gaping in the mangrove oyster, Crassostrea rhizophorae. *Comparative Biochemistry and Physiology Part A: Physiology* **93**, 395–397.

Lutterschmidt, W. I. and Hutchison, V. H. (1997). The critical thermal maximum: history and critique. *Can. J. Zool.* **75**, 1561–1574.

Ma, C.-S., Wang, L., Zhang, W. and Rudolf, V. H. W. (2018). Resolving biological impacts of multiple heat waves: interaction of hot and recovery days. *Oikos* **127**, 622–633.

Marshall, D. J. and McQuaid, C. D. (1991). Metabolic rate depression in a marine pulmonate snail: pre-adaptation for a terrestrial existence? *Oecologia* **88**, 274–276.

Marshall, D. J. and McQuaid, C. D. (2010). Warming reduces metabolic rate in marine snails: adaptation to fluctuating high temperatures challenges the metabolic theory of ecology. *Proceedings of the Royal Society B: Biological Sciences* **278**, 281–288.

McKown, J. G., Grizzle, R., Burdick, D. M., Moore, G. E., Ward, K. and White, L. E. (2025). Distribution of Rockweed Macroalgae (Ascophyllum and Fucus Spp.) and Associated Eastern Oysters (Crassostrea virginica) in the Great Bay–Piscataqua River Estuary, New Hampshire. *J Coast Res*.

McLaughlin, J. W., Bilgili, A. and Lynch, D. R. (2003). Numerical modeling of tides in the Great Bay Estuarine System: dynamical balance and spring–neap residual modulation. *Estuarine, Coastal and Shelf Science* **57**, 283–296.

McMahon, R. F. (1988). Respiratory response to periodic emergence in intertidal molluscs. *Am. Zool.* **28**, 97–114.

Meng, J., Wang, T., Li, L. and Zhang, G. (2018). Inducible variation in anaerobic energy metabolism reflects hypoxia tolerance across the intertidal and subtidal distribution of the Pacific oyster (*Crassostrea gigas*). *Marine Environmental Research* **138**, 135–143.

Michaletz, S. T. and Garen, J. C. (2024). Hotter is not (always) better: Embracing unimodal scaling of biological rates with temperature. *Ecol Lett* **27**, e14381.

Molina, A. N., Carter, M. J. and Rezende, E. L. (2024). Plasticity cannot fully compensate evolutionary differences in heat tolerance across fish species. *Evolution* **78**,.

Morgan, R., Finnøen, M. H., Jensen, H., Pélabon, C. and Jutfelt, F. (2020). Low potential for evolutionary rescue from climate change in a tropical fish. *Proc. Natl. Acad. Sci.* **117**, 33365–33372.

Nicastro, K. R., Zardi, G. I., McQuaid, C. D., Pearson, G. A. and Serrão, E. A. (2012). Love thy neighbour: Group properties of gaping behaviour in mussel aggregations. *PLOS ONE* **7**, e47382.

Nicholson, S. (2002). Ecophysiological aspects of cardiac activity in the subtropical mussel *Perna viridis* (L.) (Bivalvia: Mytilidae). *Journal of Experimental Marine Biology and Ecology* **267**, 207–222.

Oliver, E. C. J. (2019). Mean warming not variability drives marine heatwave trends. *Clim Dyn* **53**, 1653–1659.

Oliver, T. A. and Palumbi, S. R. (2011). Do fluctuating temperature environments elevate coral thermal tolerance? *Coral Reefs* **30**, 429–440.

Ørsted, M., Jørgensen, L. B. and Overgaard, J. (2022). Finding the right thermal limit: a framework to reconcile ecological, physiological and methodological aspects of CTmax in ectotherms. *Journal of Experimental Biology* **225**, jeb244514.

Ørsted, M., Jørgensen, L. B., Hůla, P. and Overgaard, J. (2025). Integrating physiological rates of thermal stress and repair predicts heat failure during temperature fluctuations.

Overton, K., Dempster, T., Swearer, S. E., Morris, R. L. and Barrett, L. T. (2024). Aerial exposure tolerance of juvenile flat oysters (*Ostrea angasi*) depends on shell length and air temperature. *Restoration Ecology* **32**, e14047.

Payne, N. L., Kong, J. D., Jackson, A. L., Bates, A. E., Morley, S. A., Smith, J. A. and Arnoldi, J.-F. (2025). Heat limits scale with metabolism in ectothermic animals. *J. Anim. Ecol.* **n/a**,.

Perdue, J. A., Beattie, J. H. and Chew, K. K. (1981). Some relationships between gametogenic cycle and summer mortality phenomenon in the Pacific oyster (Crassostrea gigas) in Washington state. *J Shellfish Res* **1**, 9–16.

Pereira, L. F., Arenas, F., Seabra, R., da Silva, R., Monteiro, C., Pereira, J., Vale, C. G., Serôdio, J., Frankenbach, S., Ghiglione, V., et al. (2025). Simulated intertidal heat stress on the brown seaweed Ascophyllum nodosum demonstrates differential population sensitivity to future climate. *J. Ecol.* **113**, 1504–1520.

Peterson, A. T., Papeş, M. and Soberón, J. (2015). Mechanistic and correlative models of ecological niches. *Eur J Ecol* **1**, 28–38.

Pörtner, H.-O., Bock, C. and Mark, F. C. (2017). Oxygen- and capacity-limited thermal tolerance: bridging ecology and physiology. *J. Exp. Biol.* **220**, 2685–2696.

Rajagopal, S., Van Der Velde, G., Jansen, J., Van Der Gaag, M., Atsma, G., Janssen-Mommen, J. P. M., Polman, H. and Jenner, H. A. (2005). Thermal tolerance of the invasive oyster Crassostrea gigas: Feasibility of heat treatment as an antifouling option. *Water Research* **39**, 4335–4342.

Raymond, W. W., Barber, J. S., Dethier, M. N., Hayford, H. A., Harley, C. D. G., King, T. L., Paul, B., Speck, C. A., Tobin, E. D., Raymond, A. E. T., et al. (2022). Assessment of the impacts of an unprecedented heatwave on intertidal shellfish of the Salish Sea. *Ecology* **103**, e3798.

Raymond, W. W., Tobin, E. D., Barber, J. S., Hayford, H. A., Raymond, A. E. T., Speck, C. A., Rogers, D. and Brown, R. (2024). Short-term effects of an unprecedented heatwave on intertidal bivalve populations: fisheries management surveys provide an incomplete picture. *Front. Mar. Sci.* **11**,.

Rezende, E. L., Castañeda, L. E. and Santos, M. (2014). Tolerance landscapes in thermal ecology. *Funct Ecol* **28**, 799–809.

Rezende, E. L., Bozinovic, F., Szilágyi, A. and Santos, M. (2020). Predicting temperature mortality and selection in natural Drosophila populations. *Science* **369**, 1242–1245.

Roesch, A. and Schmidbauer, H. (2018). WaveletComp: Computational wavelet analysis.

Sasaki, M., Isanta-Navarro, J. and Govaert, L. (2025). Experimental ecology and the balance between realism and feasibility in aquatic ecosystems. *Nature Communications* **16**,.

Schaum, C.-E., Buckling, A., Smirnoff, N. and Yvon-Durocher, G. (2022). Evolution of thermal tolerance and phenotypic plasticity under rapid and slow temperature fluctuations. *Proc Biol Sci* **289**, 20220834.

Scholkmann, F., Boss, J. and Wolf, M. (2012). An efficient algorithm for automatic peak detection in noisy periodic and quasi-periodic signals. *Algorithms* **5**, 588–603.

Seabra, R., Wethey, D. S., Santos, A. M., Gomes, F. and Lima, F. P. (2016). Equatorial range limits of an intertidal ectotherm are more linked to water than air temperature. *Glob Chang Biol* **22**, 3320–3331.

Seuront, L., Nicastro, K. R., Zardi, G. I. and Goberville, E. (2019). Decreased thermal tolerance under recurrent heat stress conditions explains summer mass mortality of the blue mussel Mytilus edulis. *Sci Rep* **9**, 17498.

Shick, J. M., Widdows, J. and Gnaiger, E. (1988). Calorimetric studies of behavior, metabolism and energetics of sessile intertidal animals. *Am Zool* **28**, 161–181.

Sibly, R. M., Brown, J. H. and Kodric-Brown, A. (2012). *Metabolic ecology: A scaling approach*. John Wiley & Sons.

Siboni, N., King, W. L., Williams, N. L. R., Scanes, E., Giardina, M., Green, T. J., Ostrowski, M., O'Connor, W., Dove, M., Labbate, M., et al. (2024). Increased abundance of potentially pathogenic Vibrio and a marine heatwave co-occur with a Pacific Oyster summer mortality event. *Aquaculture* **583**, 740618.

Smith, K. E., Burrows, M. T., Hobday, A. J., King, N. G., Moore, P. J., Sen Gupta, A., Thomsen, M. S., Wernberg, T. and Smale, D. A. (2023). Biological impacts of marine heatwaves. *Annu. Rev. Mar. Sci.* **15**, annurev-marine-032122-121437.

Smith, K. E., Aubin, M., Burrows, M. T., Filbee-Dexter, K., Hobday, A. J., Holbrook, N. J., King, N. G., Moore, P. J., Sen Gupta, A., Thomsen, M., et al. (2024). Global impacts of marine heatwaves on coastal foundation species. *Nat Commun* **15**, 1–14.

Sokolova, I. M. (2013). Energy-limited tolerance to stress as a conceptual framework to integrate the effects of multiple stressors. *Integrative and Comparative Biology* **53**, 597–608.

Sokolova, I. M., Frederich, M., Bagwe, R., Lannig, G. and Sukhotin, A. A. (2012). Energy homeostasis as an integrative tool for assessing limits of environmental stress tolerance in aquatic invertebrates. *Marine Environmental Research* **79**, 1–15.

Somero, G. N. (2002). Thermal physiology and vertical zonation of intertidal animals: Optima, limits, and costs of living1. *Integr Comp Biol* **42**, 780–789.

Somero, G. N. (2010). The physiology of climate change: how potentials for acclimatization and genetic adaptation will determine 'winners' and 'losers'. *J. Exp. Biol.* **213**, 912–920.

Stark, K. A., Clegg, T., Bernhardt, J. R., Grainger, T. N., Kempes, C. P., Savage, V., O'Connor, M. I. and Pawar, S. (2025). Toward a more dynamic metabolic theory of ecology to predict climate change effects on biological systems. *Am Nat* **205**, 285–305.

Stasse, A., Cheng, M. L. H., Meyer, K., Bumbera, N., Volkom, K. V., Laferriere, A. M., Dijkstra, J. A. and Brown, B. (2022). Temporal dynamics of eastern oyster larval abundance in great bay estuary, new hampshire. *shre* **40**, 471–478.

Steeves, L., Winterburn, K., Coffin, M. R. S., Babarro, J. M. F., Guyondet, T., Comeau, L. A. and Filgueira, R. (2025). The combined effects of temperature and exogenous bacterial sources on mortality in the Eastern oyster (Crassostrea virginica) under anoxia. *Mar Biol* **172**, 1–10.

Stillman, J. H., Amri, A. B., Holdreith, J. M., Hooper, A., Leon, R. V., Pruett, L. R. and Bukaty, B. M. (2025). Ecophysiological responses to heat waves in the marine intertidal zone. *J Exp Biol* **228**,.

Therneau, T. M., until 2009), T. L. . S.-. port and R. maintainer, Elizabeth, A. and Cynthia, C. (2026). Survival: Survival Analysis.

Truebano, M., Fenner, P., Tills, O., Rundle, S. D. and Rezende, E. L. (2018). Thermal strategies vary with life history stage. *J Exp Biol* **221**, jeb171629.

Vajedsamiei, J., Melzner, F., Raatz, M., Morón Lugo, S. C. and Pansch, C. (2021). Cyclic thermal fluctuations can be burden or relief for an ectotherm depending on fluctuations' average and amplitude. *Funct Ecol* **35**, 2483–2496.

Vajedsamiei, J., Warlo, N., Meier, H. E. M. and Melzner, F. (2024). Predicting key ectotherm population mortality in response to dynamic marine heatwaves: A Bayesian-enhanced thermal tolerance landscape approach. *Funct Ecol* **38**, 1875–1887.

van de Pol, M., Jenouvrier, S., Cornelissen, J. H. C. and Visser, M. E. (2017). Behavioural, ecological and evolutionary responses to extreme climatic events: challenges and directions. *Philosophical Transactions of the Royal Society B: Biological Sciences* **372**, 20160134.

van Heerwaarden, B. and Kellermann, V. (2020). Does plasticity trade off with basal heat tolerance? *Trends in Ecology & Evolution* **35**, 874–885.

Verberk, W. C. E. P. and Atkinson, D. (2013). Why polar gigantism and Palaeozoic gigantism are not equivalent: effects of oxygen and temperature on the body size of ectotherms. *Funct Ecol* **27**, 1275–1285.

Verberk, W. C. E. P., Overgaard, J., Ern, R., Bayley, M., Wang, T., Boardman, L. and Terblanche, J. S. (2016). Does oxygen limit thermal tolerance in arthropods? A critical review of current evidence. *Comparative Biochemistry and Physiology Part A: Molecular & Integrative Physiology* **192**, 64–78.

Verberk, W. C. E. P., Hoefnagel, K. N., Peralta-Maraver, I., Floury, M. and Rezende, E. L. (2023). Long-term forecast of thermal mortality with climate warming in riverine amphipods. *Glob Chang Biol* **29**, 5033–5043.

Villeneuve, A. R. and White, E. R. (2024). Predicting organismal response to marine heatwaves using dynamic thermal tolerance landscape models. *Journal of Animal Ecology* **94**, 1515–1527.

Villeneuve, A. R., Komoroske, L. M. and Cheng, B. S. (2021). Diminished warming tolerance and plasticity in low latitude populations of a marine gastropod. *Conserv Physiol* **9**, coab039.

Walton, L. N., Watts, V. R., Schuster, J. M. and Bates, A. E. (2025). Cool ocean temperatures offer limited protection to a heat-stressed keystone predator during atmospheric heatwaves. *Mar. Ecol. Prog. Ser.* **773**, 77–93.

Wendling, C. C. and Wegner, K. M. (2013). Relative contribution of reproductive investment, thermal stress and *Vibrio* infection to summer mortality phenomena in Pacific oysters. *Aquaculture* **412–413**, 88–96.

Wernberg, T., S. Thomsen, M., K. Baum, J., J. Bishop, M., F. Bruno, J., A. Coleman, M., Filbee-Dexter, K., Gagnon, K., He, Q., Murdiyarso, D., et al. (2024). Impacts of climate change on marine foundation species. *Ann Rev Mar Sci* **16**, null.

White, R. H., Anderson, S., Booth, J. F., Braich, G., Draeger, C., Fei, C., Harley, C. D. G., Henderson, S. B., Jakob, M., Lau, C.-A., et al. (2023). The unprecedented Pacific Northwest heatwave of June 2021. *Nat Commun* **14**, 1–20.

Xu, T., Newman, M., Capotondi, A., Stevenson, S., Di Lorenzo, E. and Alexander, M. (2022). An increase in marine heatwaves without significant changes in surface ocean temperature variability. *Nature Communications* **13**,.

Zwaan, A. de and Eertman, R. H. M. (1996). Anoxic or aerial survival of bivalves and other euryoxic invertebrates as a useful response to environmental stress—A comprehensive review. *Comparative Biochemistry and Physiology Part C: Pharmacology, Toxicology and Endocrinology* **113**, 299–312.

13 Figure legends

Figure 1. Conceptual figure of predicting survival in the intertidal eastern oyster *Crassostrea virginica* in a single tidal cycle. A tide cycle is defined as starting with immersion and ending immediately after a full immersion-emersion cycle. A) A tidal height time series and corresponding temperature logger tide height are used to delineate periods of submersion and exposure (immersion and emersion). B) These periods of logger submersion are converted to an exposure status for observed intertidal temperature taken from a data logger. C) and D) represent the thermal death time (TDT) curves for oysters submerged in water (immersion at high tide, blue) and exposed to air (emersion at low tide, red). These curves are then used as the basis for a probabilistic Thermal Tolerance Landscape (TTL) for each exposure type. E) Each exposure TTL is then used to calculate cumulative survival conditionally based on the exposure status of each temperature observation. We finally calculate the survival of oysters across multiple tide cycles to produce a prediction of cumulative survival over time in the intertidal.

Figure 2. Thermal Death Time (TDT) curve for adult *C. virginica* exposed to air and water immersion heat stress. Thermal Death Time (TDT) curve for adult *C. virginica* exposed to air and water immersion heat stress. Ribbons around lines of fit are confidence intervals. Dashed line of fit describes the model when extrapolated beyond bounds of time to death data collected. Inset table contains TDT parameters, including R^2 (goodness of fit between the parameterized TDT curve and raw data), CT_{max} (acute thermal tolerance, x intercept when y = 1 min), and z (chronic thermal tolerance, slope of line). Standard error around CT_{max} and z were propagated with Taylor series expansion via the Delta method from linear model fit parameters (see Methods). The black point and dashed lines indicate the point of TDT curve intersection at 37 °C and 1,941 minutes.

Figure 3. Intertidal temperatures at Brackett's Point and JEL, with corresponding observed and modeled survival under original TTLs. A) Intertidal temperature in the upper intertidal of Brackett's Point between May 16th and September 10th 2025 (left panel) and Jackson Estuarine Lab (JEL; right panel) between May 29th and September 9th 2025, co-located with oyster mortality survey. Red portions of the time series indicate time stamps when the loggers (and by proxy, the field deployed oysters) were predicted to be above water (low tide, exposed status), blue portions when loggers were predicted to be below water (high tide, submerged status). B) Field observed survival (points), 95% CI of field survival (colored ribbon), and modeled survival of 83 oysters distributed across Brackett's Point and JEL. The line type indicates the type of survival prediction, with the dashed line representing field survival, the dotted black line the

survival prediction given by the experimental data, and the multiple solid lines indicating the 100 bootstrapped survival predictions from the original survival model.

Figure 4. Survival predictions using simulation calibrated TTLs. A) Survival predictions produced from 81 different TTL parameter combinations (gray), with the best-fit model to field data (red) highlighted in blue. The colored ribbons indicate the 95% confidence interval around percent change in field survival. Modeled survival prediction using experimentally-derived TTLs shown in black. B) Percent change analysis used to identify the optimal combination of TTL parameters to minimize Root Mean Squared Error between predictions (gray lines) and field data (red lines and points). Black lines and points indicate modeled survival using experimentally-obtained TTLs. The percent change in survival given by the combination of TTL parameters that minimized RMSE are shown in blue. For field data from JEL, the two extreme mortality observations that were not attributable to heat stress and removed from percent change analysis and the final selection of the optimal TTL parameter combination are shown in dotted red lines.

Figure 5. Impacts of 2° C warming on modeled intertidal oyster survival. Impacts of 2 °C warming during tidal emersion (yellow), immersion (green), and throughout the tidal cycle (red) on predicted oyster mortality at Brackett's Point and JEL. Warmer water had the smallest impact on oyster survival, with warming in both air and water having the largest impact on survival due to the relatively larger contribution of warmer emersion to mortality.

Figure 6. Conceptual diagram of the proposed physiological, physical, and behavioral drivers of immersed and emersed TDT curves. At lower lethal temperatures, immersed oysters (blue) may die due to starvation and increased susceptibility to bacterial infection, increasing demands on energy for basic maintenance. Emersed oysters (red) experience desiccation stress over long periods of time, impacting their ability to exchange gases across tissues and perform other organ functions. Over higher lethal temperatures, immersed oysters may die due to an insufficient supply of dissolved oxygen, inability to behaviorally thermoregulate via gaping, and lack of an environmental signal to induce cellular defenses. Finally, emersed oysters may depress their metabolism and upregulate cellular defenses in response to an emersion environmental signal, thereby extending their time to death compared to immersed counterparts. They additionally may gape, which can increase oxygen availability for aerobic metabolism as well as cooling the individual through evaporation. Not shown are molecular processes such as protein denaturation and loss of membrane layer integrity.

Supplementary Materials and Methods 1 Further Experiment Methods

Supplementary Materials and Methods 1.1 Oysters for the Immersed Thermal Death Time Experiment

We collected 300 adult NEH line diploid Eastern oysters (*Crassostrea virginica*) from Fox Point Oysters, an aquaculture site located in Great Bay, New Hampshire, USA (43°07'45.6"N, 70°51'03.6"W), for use in immersion experiments. Oysters were at least one year old, and seed was originally sourced from Muscongus Bay Aquaculture. We transported 50 oysters from the farm on May 9th, 2024, and 250 more on June 28th, 2024, to the University of New Hampshire's Coastal Marine Lab (CML), located in New Castle, NH, USA (43°04'18.6"N, 70°42'37.3"W). We kept experimental oyster stock in a 300-liter flow-through circular tank with airstones, so that oysters were able to filter feed from the raw seawater. Starting on July 11th 2024, we began daily water changes to remove sediment from the tank, and every three days, we provided supplementary feeding of concentrated shellfish diet (Shellfish Diet 1800, Reed Mariculture Inc, Campbell, CA). We monitored water parameters (temperature, dissolved oxygen, salinity, and pH) with a YSI meter (ProfessionalPlus Multiparameter Meter, Yellow Springs Instruments, Yellow Springs, OH, USA), and ammonia and nitrate using saltwater test kits (API Fish Care, Chalfont, PA, USA). Ammonia levels never exceeded 0.25 ppm, and nitrate levels never exceeded 5 ppm. Additionally, we continuously recorded water temperature in the flow-through tank with a HOBO logger every 15 minutes (HOBO Tidbit MX, Onset Corporation, Onset, MA, USA). Oysters acclimated to the flow-through seawater lab conditions for at least ten days before they were selected for experimentation.

Water temperatures in the flow-through CML seawater system averaged 14.7 °C (2.2 °C SD) during the experimentation period (May 9th-September 9th 2024), whereas water temperature in Great Bay, NH (National Estuarine Research Reserve System (NERRS) Buoy GRBGWQ) averaged 20.4 °C (2.7 °C SD). Temperatures in mid-May in Great Bay, where oysters originated, were 15 °C, rising to 17 °C by June. Thus, the average temperatures in the CML acclimation tank replicated late spring conditions in Great Bay. Due to an increase in mean temperature in the flow-through CML seawater system in August (August mean 17 °C) as the intake seawater warmed, some experimental trials were conducted with oysters who had acclimated at a slightly warmer temperature than earlier trials. We included a two-week mean acclimation temperature parameter in our exploratory model selection. However, exploratory analysis revealed no effect of acclimation on time to death and we removed acclimation as a potential covariate term (Appendix Supplementary Materials and Methods 2). Salinity in the CML holding tank averaged 31.4 (0.5 SD) PSU in July and August, which was close to conditions in Great Bay during the same time period (> 28 PSU), but more saline than conditions during the mid-May collection (≈ 20 PSU).

300-watt heaters maintained water temperatures within each individual tank using feedback from individual temperature probes. Dissolved oxygen was recorded with Oxyguard oxygen probes (Neptune Systems, Morgan Hill, CA), but only in the top five experimental tanks. Dissolved oxygen

decreased with increasing experimental temperature during experiments, with average values ranging from 22.6% (40°C) to 67.7% (32° C), but large variability at higher temperatures (Table S6). We did not bubble air into tanks to more closely replicate environmental conditions. In order to avoid build-up of ammonia and nitrate from waste products and oyster death, we used peristaltic pumps (DOS Pump, Neptune Systems, Morgan Hill, CA) to pump 115 liters/day/tank of pre-heated water from the bottom sump tanks to the top experimental tanks. The water flow into each tank was further split using a four-way manifold to four smaller tanks (4.7 liters) housing individual oysters. Thus, each large 80 liter tank (one temperature treatment) served as a waterbath for the four smaller tanks. We pumped 29 liters/day of pre-heated seawater into each subtank, resulting in more than six full volume replacements per day. The standpipe of each waterbath maintained the water bath level just below the lip of each sub-tank, so that used water overflowed each sub-tank.

Temperature in sub-tanks remained stable due to the pre-heating of fresh seawater and conduction from the heated water bath. We recorded temperature using either the recorded temperature from the APEX temperature probe or from a thermocouple probe (TC-08 Data Logger and type T thermocouples, Omega Technology, Tyler, TX, USA).

In total, we conducted eight experimental runs of the immersed experiment. We collected time to death data for 150 oysters, of which we analyzed 139. One oyster was removed from analysis a priori from the first experiment due to a significantly larger shell size and mass than others used in our experiments.

Supplementary Materials and Methods 1.2 Oysters for the Emersed Thermal Death Time Experiment

We conducted experiments building a low tide, air-exposed *C. virginica* thermal death-time (TDT) curve in fall of 2024, again we obtained 100 oysters from Fox Point Oysters. We acclimated oysters in a 568-liter indoor recirculating seawater system for at least one week prior to experimentation, with a chiller setpoint of 15 °C (15.2 °C, 0.96 SD) to match the average acclimation temperature of oysters in the immersed TDT experiment. We maintained salinity at 31 PSU using filtered seawater obtained from CML. Oysters were fed at least every three days (Shellfish Diet 1800, Reed Mariculture Inc, Campbell, CA), and we also changed the water every three days. Ammonia levels never exceeded 0.25 ppm, and nitrate levels never exceeded 5 ppm. Additionally, water temperature in the flow-through tank was recorded continuously with an ElectricBlue temperature logger every 15 minutes (T7.3 Envlogger, ElectricBlue, Porto, Portugal).

Supplementary Materials and Methods 1.3 Oyster Preparation

We measured and weighed oysters selected for experimentation using an analytical balance and digital calipers. Average shell mass across immersed treatments was 40.9 g (7.0 g SD), and average shell height was 75.2 mm (7.4 mm SD), and in the emersed treatments the average shell mass was 20.0 g (4.8 g SD) with an average shell height of 61.0 mm (5.4 mm SD; Table S1). Because oyster

sizes between experiments were different due to availability, we included size as a covariate in later models.

We used two ElectricBlue PULSE V2 (ElectricBlue CRL, Porto, Portugal) heart frequency loggers to amplify and record infrared signals from Vishay CNY70 optical infrared sensors (Vishay Intertechnology, Inc, Malvern, PA, USA). Infrared detection of heart beats relies on infrared (IR) light-emitting diode sensors with a dual emitter and phototransistor to record reflected light. By detecting changes in reflected light when positioned over a heart, the PULSE unit records the fluctuations as an electric signal that can be saved on an SD card for later processing (Abbas et al., 2024; Burnett et al., 2013; Levinton et al., 2020; Lima et al., 2025). The PULSE unit was set to record data at 20Hz (5ms intervals).

We used a rotary tool (WEN 23190, WEN Products, Elgin, IL, USA) with a sanding attachment to grind a hole directly above the heart in the left (cupped) valve, as the shell of *C. virginica* is generally too thick to allow for sufficient IR transmission and reflection back to the sensor. We located the approximate location of the heart on each oyster by identifying the normal height axis of the left valve and its intersection with the primary ridge closest to the umbo, generally occurring around one third of the shell height from the umbo. We drilled a circular hole no larger than 5 mmin diameter and allowed drilled oysters to recover in ambient seawater for at least 24 hours prior to experimentation. Of the 300 oysters used for submerged thermal stress experiments, 22 drilled oysters and 21 undrilled oysters died over the course of the summer in the acclimation holding tank, and of the 100 oysters used in exposed experiments, 4 undrilled and no drilled oysters died. This method appears to have little effect on oyster survival, with previous experiments maintaining drilled oysters for many months (Bakhmet et al., 2015; de Carvalho et al., 2022; Federighi, 1929; Feng, 1965; Feng and Van Winkle, 1975; Koehring, 1937). After at least 24 hours, we checked for oyster heart rate using a PULSE unit, and if a strong signal was found, we selected the oyster for experimentation.

Supplementary Materials and Methods 1.4 Submerged and Exposed Experimental Design

For the immersed experiment, we exposed oysters to chronic, static water temperatures in a flow-through experimental seawater system at CML. The system is composed of ten insulated ABS tanks (80L capacity) in a 2 x 5 configuration. Tanks in the top row were used as experimental tanks, while bottom tanks acted as a pre-heated water sump for each top tank. We used an internet-connected, system-wide control system (APEX, Neptune Systems, Morgan Hill, CA, USA) to monitor and control water quality parameters through connected heat bars (Energy Bar 832, Neptune Systems, Morgan Hill, CA, USA). We were limited to 20 oysters per experimental trial (10 in the case of our first submerged trial) due to the PULSE units having capacity for ten channels each (Table S5). Therefore, we conducted a series of sequential, time-blocked trials in order to obtain desired sample sizes. While thermal death time curves generally follow a log-linear relationship with temperature, extrapolating time to death data to higher or lower temperatures can be error-prone (Jørgensen

et al., 2019). Therefore, we varied assay temperatures between trials to collect time to death data across a broad temperature gradient given our sample size limitations within each experiment. We also recorded dissolved oxygen, salinity, and pH with a YSI probe and Ammonia and Nitrate via kits in one subtank containing a living oyster per temperature treatment each day (Figure S12; Figure S13). We ended the trial once all oysters had died (determined by both referring to heart rate data and manual manipulation of shells) across treatments.

For the emersed trial, we used a pair of heated incubation chambers (Insect Rearing Chamber IN03, Darwin Chambers, St. Louis, MO, USA) to create static aerial temperature treatments. We maintained mean humidity levels between 68-72% by filling a tray of reverse-osmosis freshwater at the bottom of each chamber. These humidity levels approximate intertidal humidity levels in Great Bay, which are between 50-90% (Cheng et al, unpublished data). We recorded chamber temperature and humidity levels with separate digital loggers and with probes in a glycol solution (GSP-6G, Elitech Technologies, San Jose, CA, USA; Figure S14).

Supplementary Materials and Methods 2 Exclusion of acclimation from models

Two-week acclimation temperature prior to experimentation differed between experiments in the submerged exposure experimental set, motivating us to perform model selection and analysis with an acclimation covariate. The most parsimonious model had an interaction between temperature and acclimation on the response of time to death in the immersed experiment. The basic temperature, additive acclimation, and interactive acclimation models for the emersed experiment all had the same ΔAIC, and thus we decided to select the simplest model (Table S1).

From this best model, we found strong support for the interactive effect ($P = 0.003$) of temperature and acclimation exposure on time to death (Gaussian Linear Model, $F_{3,76} = 117.76$, $R^2 = 0.823$, Table S2). From these model parameter estimates, increasing assay temperature decreases log 10 time to death, and increasing acclimation temperature results in faster death at lower temperatures, but at acute exposures survival is longer than oysters from a cooler acclimation. However, based on our experimental design, we only had oysters emersed to the warmer 16°C acclimation in assay temperatures between 32-40 °C, while we had experiments with 13°C acclimated oysters emersed to assays between 32-46°C. Thus, the acclimation-interactive model risks extrapolation outside of the assay values for 16°C acclimated values (40-46°C), and when the model is re-run over overlapping assay temperature values (32-40°C) acclimation was no longer a significant interactive term ($P = 0.418$). We therefore removed all candidate models with acclimation covariate terms in our final round of model selection (see main text).

Supplementary Materials and Methods 3 Wavelet Analysis Methods and Examples

WaveletComp uses Morlet wavelets to analyze non-stationary time series for changes in periodicity and frequency through time. Alternative heartbeat detection using local maxima or Fourier transforms are difficult for non-stationary cardiac frequency data, as was the case in our lethal exposure experiments. The PULSE unit uses infrared reflectance as a proxy for cardiac activity, rather than a direct measure of cardiac activity using electrocardiograms. Therefore, subtle changes in anatomical positioning of oyster tissue during the experiment can further change the strength of the observed signal. Prior to conducting a wavelet analysis, we used a low-pass sixth-order Butterworth filter from the `signal` package to smooth the signal and emphasize the QRS components of the heartbeat (Ligges et al., 2024). We set the time resolution of our analysis to one second (data recorded at 20 Hz), and the frequency resolution at 1/20. We examined periods in our data series ranging from 0.5 to 60 seconds. Data were detrended by the built-in oscilloscope within the PULSE unit. We visualized and saved hourly wavelet spectrum plots as individual files for each channel to allow for manual inspection of heart signals. Due to the volume of data, we used the University System of New Hampshire's Premise HPC cluster with support from the Research Computing Center to perform wavelet analyses.

Below, we provide examples of 1) normal oyster cardiac activity, 2) cardiac activity at death, 3) intermittent cardiac activity prior to death, 4) signal noise/non-cardiac signal, and 5) validation of manually extracted death times using moving-window of signal variation.

Figure S1 is an example baseline signal where the oyster is alive and heart is beating over an hour of data collection. Note the two periods of the signal between 0.5 and 1 seconds. The corresponding raw signal for the same oyster, trial, and hour but over the first five minutes is found in Figure S2.

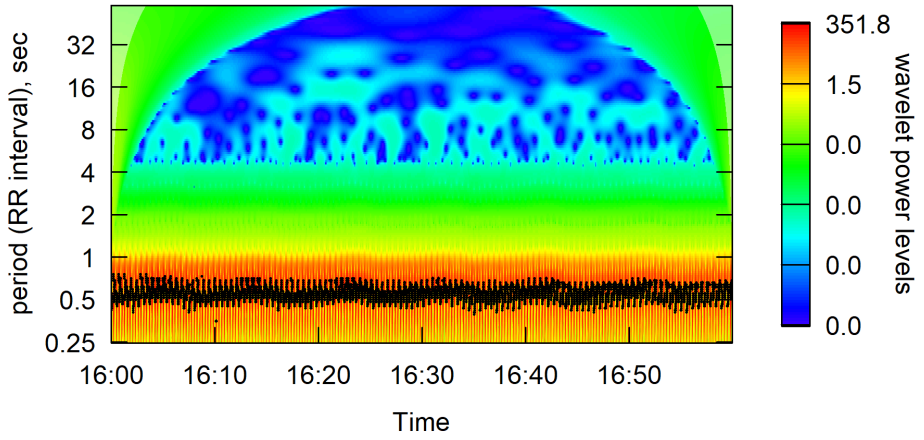

Figure S1: Wavelet analysis of submerged Oyster 9 in trial 3, 34 C, hour 7

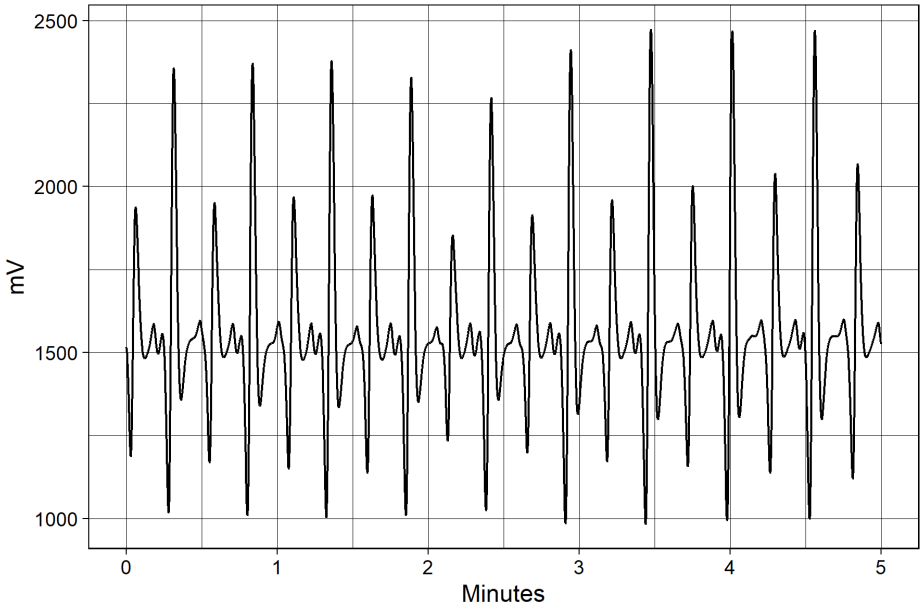

Figure S2: Raw cardiac activity of submerged Oyster 9 in trial 3, 34 C, hour 7.

Figure S3 and Figure S4 represent typical behavior of oyster cardiac activity close to death. In Figure S4 we see a very clear point of death at 35 minutes when the last heart beat peak is observed. Note the milivolt range of these signals are much smaller than those occurring in the normal heart rate.

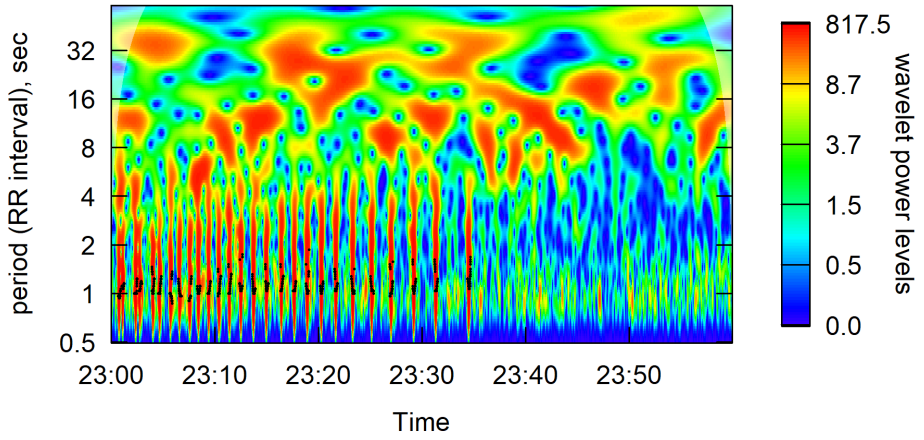

Figure S3: Wavelet analysis of submerged Oyster 9 in experiment 3, 34 C, hour 38

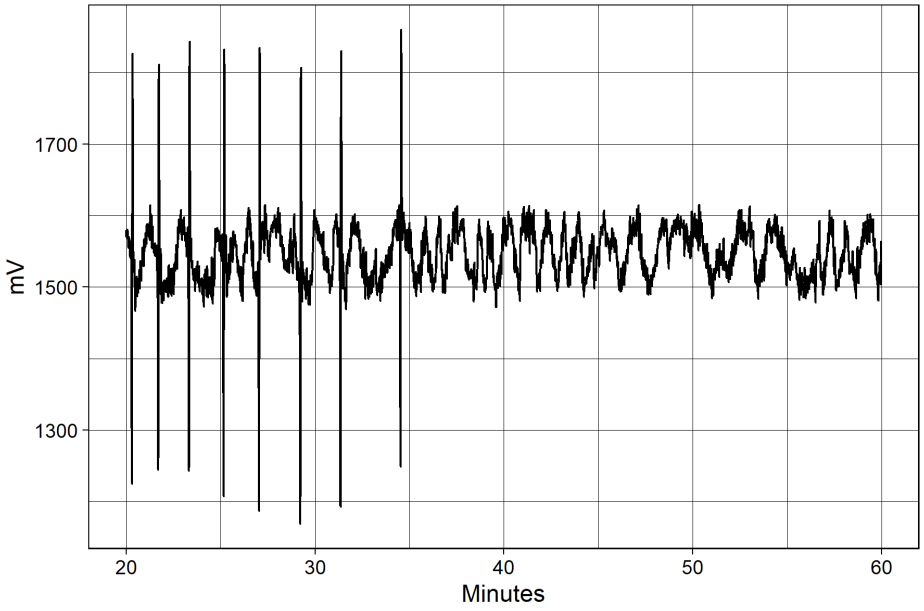

Figure S4: Raw cardiac activity of submerged Oyster 9 in experiment 3, 34 C, hour 38

In many cases, we would observe the rapid loss of consistent heart signal as shown above, but it would be followed by a few hours of inconsistent QRS signals. These heartbeats are likely a spasm response that accompanies near-lethal conditions, or bradycardia. Figure S5 shows the wavelet plot for oyster 1, trial 1, at hour 34 in the 37°C treatment, with corresponding raw signal for the same period (the full hour) in Figure S6.

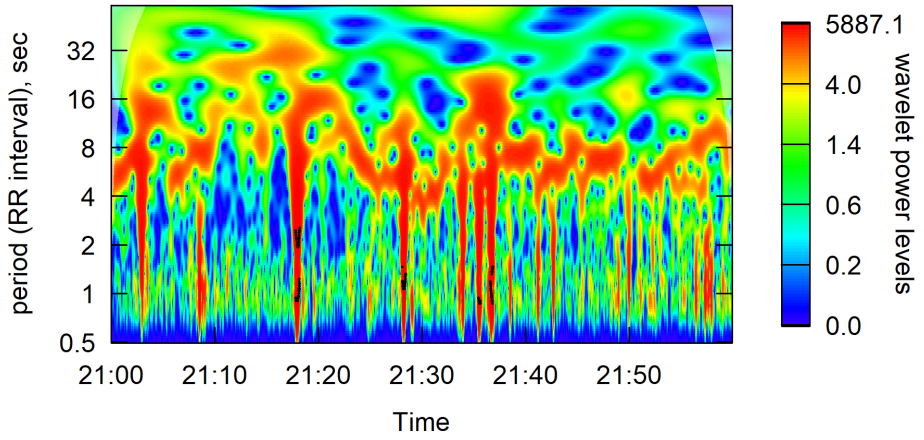

Figure S5: Wavelet analysis of submerged Oyster 1 in trial 1, 37 C, hour 34 – an example of bradycardia prior to death.

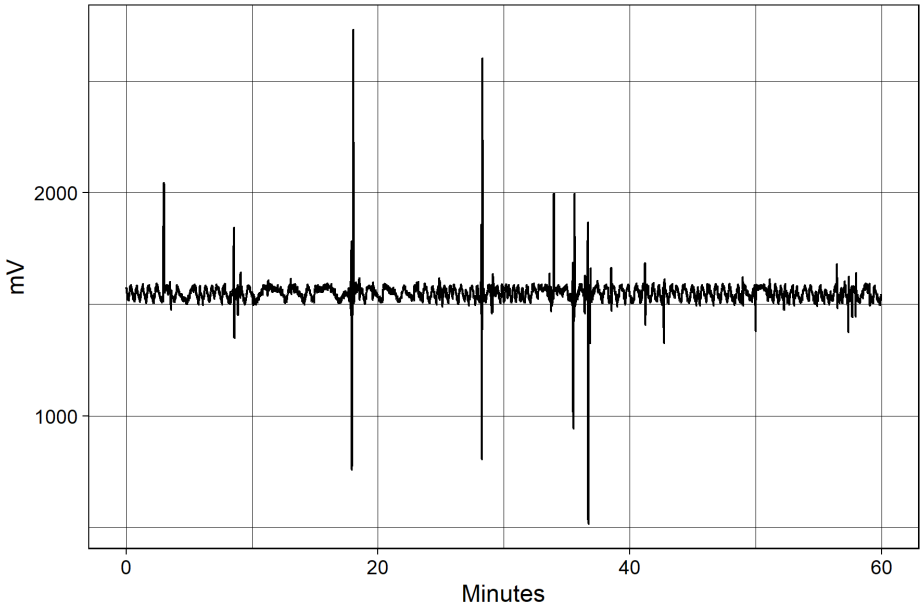

Figure S6: Raw cardiac activity of submerged Oyster 1 in trial 1, 37 C, hour 34 – an example of bradycardia prior to death.

In some cases, what appear to be heart beat signals were actually movement of dead tissue from the peristaltic pump we used to exchange stale seawater with pre-heated fresh seawater in each treatment bath. Below is an example as both a wavelet figure and raw data - note that there is no descending peak before or after the ascendant peak. Further, notice that the range of values

on the raw data is quite low. The larger periods are an artifact of the Pulse unit itself, while the smaller (40 mv) values are the fluctuations that appear in the wavelet power image.

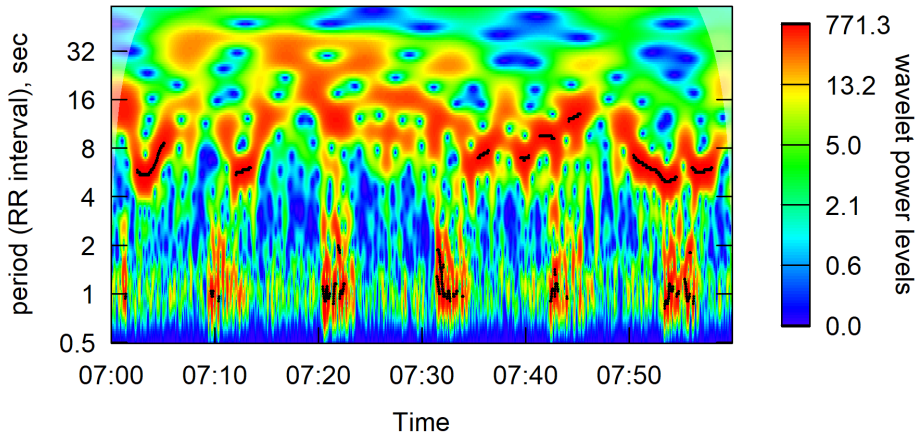

Figure S7: Wavelet analysis of signal noise in submerged Oyster 18 in trial 4, 40 C, hour 45.

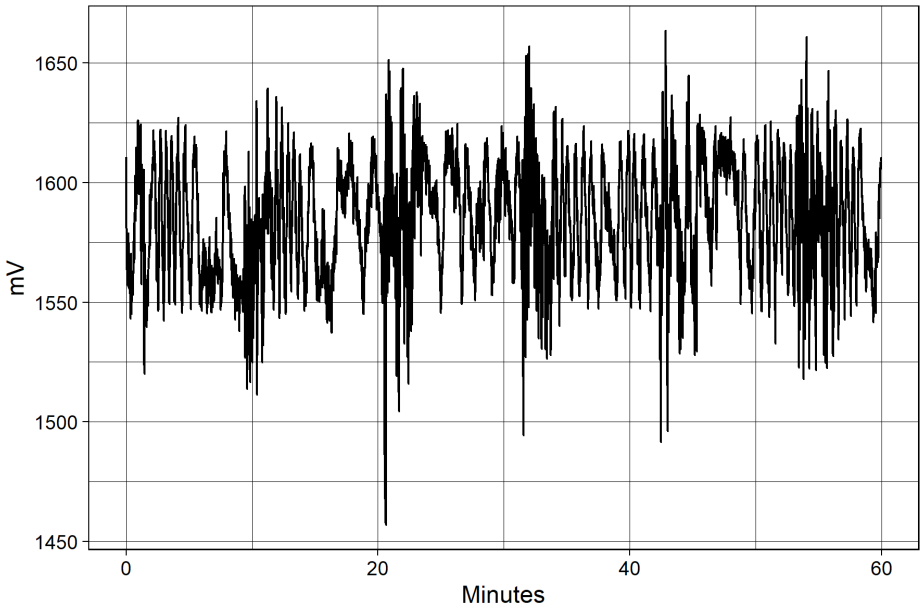

Figure S8: Signal noise in submerged Oyster 18 in trial 4, 40 C, hour 45

In addition to recording time to death as a result of collapse of the wavelet function, we also plotted this time to death against a rolling ten second window of the standard deviation in cardiac activity. Doing so demonstrated two things 1) The infrequent absence of breakpoints in rolling SD

analysis that could be used for automated point of death detection, and 2) the close agreement of visually-extracted time of death from wavelet plots and rolling window SD analysis.

As an example, we analyze below the rolling window SD of an oyster that died quickly at 48 C. The vertical red line indicates the extracted time of death from wavelet analysis.

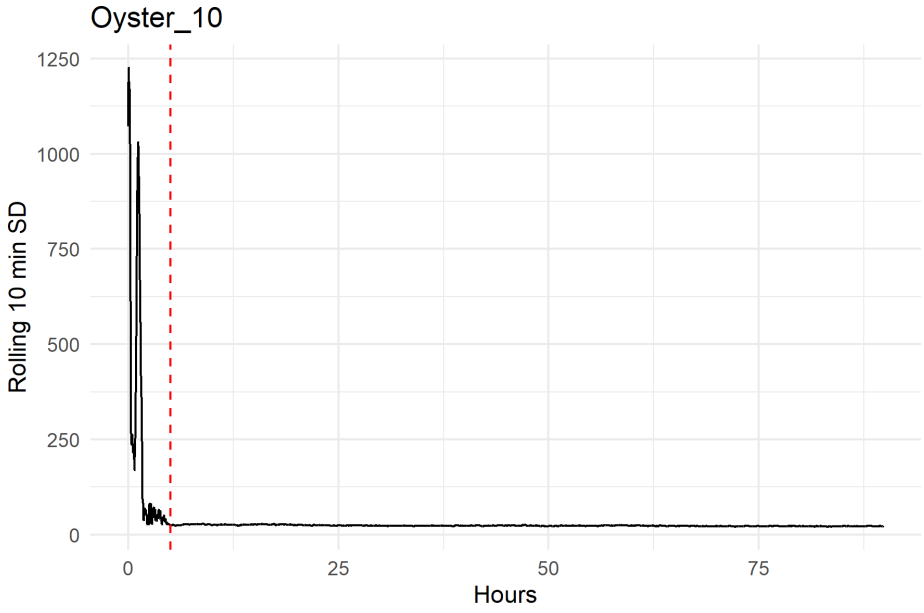

Figure S9: Rolling Window analysis of cardiac activity SD in exposed Oyster 10 in trial 7, 48 C. Vertical red line indicates the extracted time of death from wavelet analysis

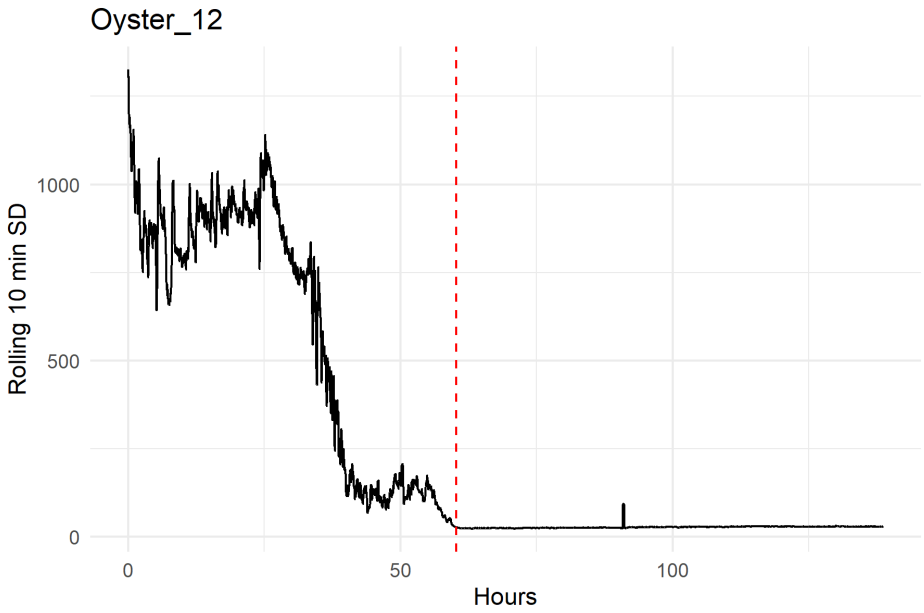

Figure S10: Rolling Window analysis of cardiac activity SD in exposed Oyster 12 in trial 7, 34 C. Vertical red line indicates the extracted time of death from wavelet analysis

A final example is oyster 14 in trial 4, which demonstrates how the exact time where the rolling window SD plateaus can be obscured by signal noise.

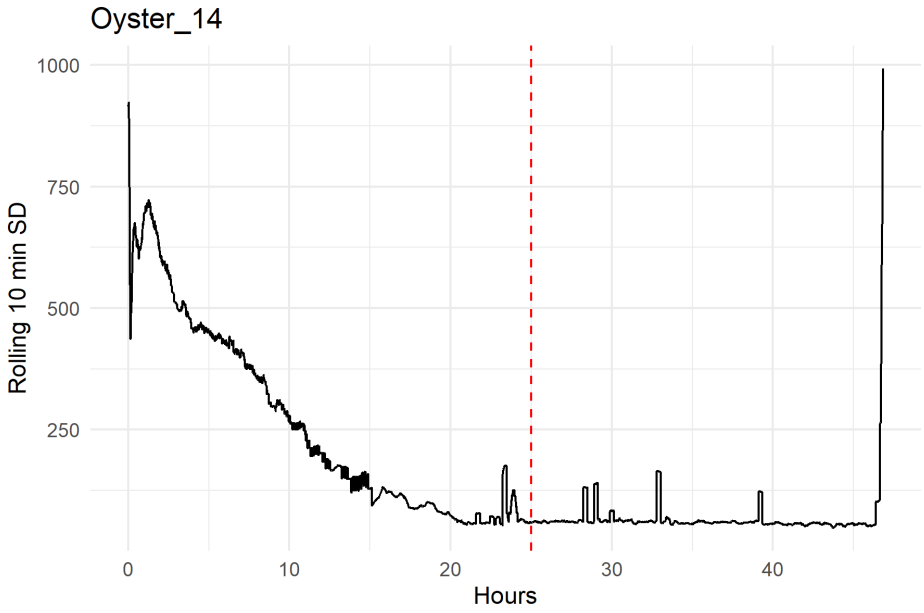

Figure S11: Rolling Window analysis of cardiac activity SD in submerged Oyster 14 in trial 4, 38 C. Vertical red line indicates the extracted time of death from wavelet analysis

Supplementary Materials and Methods 4 Tide Height Code Functionality

To determine the immersion regime of the field intertidal temperature logger, we built a function to extract the tidal height of the logger and apply an interpolated time series of immersion/emersion status to the measured intertidal temperature. We first identified logger immersion points, diagnostic as precipitous drops of at least 3 °C/15 min from temperature peaks that occur during summer low tide events (Gilman et al., 2006; Harley and Helmuth, 2003). In addition to manually scoring immersion points, we used Automatic Multiscale-based Peak Detection (AMPD) algorithms (Scholkmann et al., 2012), immersion points based on both threshold and first-derivative detection in water pressure logger data from both sites, and finally manual scoring of water pressure logger data. Because we were unable to deploy the water pressure loggers for the duration of the field experiment, we were not able to use the raw immersion times themselves as our basis for immersion point scoring. Due to the protected and enclosed nature of Great Bay, there is minimal wave splash at the study location. Therefore, we did not calculate a wave splash correction factor for our logger immersion events.

To determine the immersion regime of temperature loggers in Great Bay, we developed a custom R function, `tide_findR`, to estimate the local tide height and time offset from the nearest available tide station (43°03'11"N 70°54'46"W, NOAA Station 8422687, Squamscott River RR Bridge, NH, USA) located 3.6 km and 5.9 km up-estuary from Brackett's Point and JEL, respectively. We used XTide (www.flaterco.com) to acquire the subordinate tide series at Squamscott River during the field deployment period. Since tidal height and timing can vary spatially, this adjustment was necessary to align logger immersion events with the local tidal cycle. The code behind `tide_findR` can be found in the accompanying anonymized code repository: https://anonymous.4open.science/r/oyster_TDT_manuscript2026-5F07

First, the function shifts the reference tide series forward in time, extracting tide heights corresponding to each recorded immersion timestamp. At each shift, the function calculates the sum of squared differences (least squares) between observed immersion heights and the mean tide height. The time offset that minimizes the least squares is selected as the best estimate of the logger's time shift relative to the reference tide station.

Using this optimal time shift, the function assigns a tide height to each immersion timestamp and calculates a mean logger height, representing the submergence threshold. This threshold is then used to classify each temperature observation as submerged (immersed) or exposed (emersed), providing a time series of temperature data linked to tidal exposure. We then used identified which immersion detection methods minimized sum of squares for each site. We ultimately selected the manual scoring method of immersion from water pressure logger data for both sites, as the this method had one of the smallest minimized sum of squares and was the most proximate measure of immersion timing (compared to temperature drops). We therefore used the calculated time offset and tide height using this method to categorize each temperature observation from the intertidal

temperature loggers as immersed or emersed.

Due to the complex hydrodynamics of the Great Bay estuary, a single time offset and tide height threshold sometimes incorrectly classified temperature points as immersed or emersed (McLaughlin et al., 2003). This was more noticeable at JEL, where water funnels through the narrow Furber Strait (300 m wide), resulting in more complex water level heights than predicted at the Squamscott River tide station or observed at Brackett's Point.

Model	K	AIC_c	ΔAIC_c	AIC Weight	Log Likelihood
$\log_{10}(min.of.death) \sim temp \times type$	**5**	**66.13**	**0**	**0.52**	**-27.84**
$\log_{10}(min.of.death) \sim temp + mass_g \times type$	*6*	*66.26*	*0.13*	*0.48*	*-26.81*
$\log_{10}(min.of.death) \sim temp + type$	5	97.45	31.33	0	-43.5
$\log_{10}(min.of.death) \sim temp + mass_g + type$	6	97.47	31.34	0	-42.42
$\log_{10}(min.of.death) \sim temp \times type + acc$	7	99.67	33.54	0	-42.41
$\log_{10}(min.of.death) \sim temp + mass_g \times type + acc$	5	105.86	39.73	0	-47.71
$\log_{10}(min.of.death) \sim temp + type + acc$	4	107.21	41.09	0	-49.46
$\log_{10}(min.of.death) \sim temp + mass_g + type + acc$	6	107.99	41.86	0	-47.68

Table S1: Model selection outputs for TDT experiments with acclimation covariates. Bold face font indicates model selected under AIC, italic face font indicates which model was used in the final analysis (see main text).

	Estimate	Standard Error	t-value	P value
Intercept	21.815	4.303	5.07	**<0.0001**
Temperature (°C)	-0.517	0.116	-4.459	**<0.0001**
Acclimation (°C)	-0.909	0.311	-2.923	**0.00456**
Temperature * Acclimation	0.026	0.008	3.052	**0.00313**

Table S2: Model summary of the interactive temperature-acclimation TDT model for the immersion experiment. We rejected this model despite the lower AIC value due to parameter significance arising only from non-overlapping temperature treatments. Bold font indicates P values < 0.05.

Experiment	Exposure	Height (mm) mean	Height (mm) SD	Weight (g) mean	Weight (g) SD
exp_1	immersed	73.14	7.18	38.13	5.42
exp_2	immersed	72.31	5.87	41.60	5.65
exp_3	immersed	74.69	6.14	43.11	7.45
exp_4	immersed	82.19	6.32	43.15	8.68
exp_5	emersed	60.50	6.44	20.13	5.49
exp_6	emersed	61.17	5.70	20.20	3.29
exp_7	emersed	61.29	4.05	19.86	5.63
pilot	immersed	82.39	7.68	52.47	20.90

Table S3: Mass and height of oysters used across emersed and immersed TDT experiments.

Measurement	Exposure	Estimated Marginal Mean	SE	Lower CI	Upper CI
Mass (g)	emersed	20.06	1.35	16.64	23.49
Mass (g)	immersed	41.85	1.11	39.16	44.54
Height (mm)	emersed	60.99	2.38	55.09	66.88
Height (mm)	immersed	76.37	1.88	71.79	80.95

Table S4: Estimated Marginal Means of oyster mass and height across exposure experiments. EMMs performed over mixed-effects linear models of height or mass as a function of experiment exposure type, with experiment time block as the random effect (1|experiment).

Experiment	Start Date	End Date	Experiment Duration (days)	Assay Temperature (°C)	Number of Oysters	Analyzed Oysters	Temperature Source	Exposure
pilot	7/2/2024 11:00	7/3/2024 10:00	0.96	43, 46	10	8	apex	submerged
exp_1	7/15/2024 13:00	7/18/2024 9:00	2.88	37, 40, 43, 46	20	19	apex	submerged
exp_2	7/23/2024 9:15	8/6/2024 9:00	14.00	32, 34, 36, 38, 40	20	18	apex	submerged
exp_3	8/6/2024 10:00	8/19/2024 9:00	12.96	32, 34, 36, 38, 40	20	15	apex	submerged
exp_4	8/22/2024 13:00	9/9/2024 10:00	17.88	32, 34, 36, 38, 40	20	19	pico	submerged
exp_5	11/20/2024 9:45	11/23/2024 0:00	2.59	40, 46	20	20	elitech	exposed
exp_6	12/3/2024 11:30	12/9/2024 10:30	5.96	37, 43	20	20	elitech	exposed
exp_7	12/12/2024 14:30	12/18/2024 10:30	5.83	34, 48	20	20	elitech	exposed

Table S5: Table of thermal death time experiment metadata across immersed and emersed experiments. We only used ten oysters in the first experiment due to the availability of a single PULSE unit. Duration reflects the length of time the experiment was running until the last oyster died and was not chosen *a priori*.

Table S6: Summary statistics of experimental treatment temperatures used in TDT experiments across exposures.

Treatment (°C)	Mean (°C)	SD (°C)	Lower CI	Upper CI	Experiment	Temperature Probe Source	Exposure
43	43.01	0.23	42.98	43.05	pilot	apex	Immersed
46	45.75	0.46	45.68	45.81	pilot	apex	Immersed
37	37.34	0.48	45.03	45.04	exp_1	pico	Immersed
40	41.45	1.26	37.34	37.34	exp_1	pico	Immersed
43	45.04	1.17	41.44	41.45	exp_1	pico	Immersed
46	48.02	0.64	48.02	48.03	exp_1	pico	Immersed
37	36.81	0.18	42.46	42.54	exp_1	eb	Immersed
40	40.12	0.45	36.82	36.89	exp_1	eb	Immersed
43	42.52	0.33	40.07	40.14	exp_1	eb	Immersed
46	44.82	0.63	44.78	44.86	exp_1	eb	Immersed
37	37.01	0.53	42.83	42.91	exp_1	apex	Immersed
40	40.08	0.45	36.97	37.04	exp_1	apex	Immersed
43	42.87	0.38	40.05	40.11	exp_1	apex	Immersed
46	45.14	0.66	45.09	45.18	exp_1	apex	Immersed
32	32.89	0.74	32.89	32.89	exp_2	pico	Immersed
34	34.08	0.78	34.08	34.08	exp_2	pico	Immersed
36	37.47	0.65	37.47	37.47	exp_2	pico	Immersed
38	39.15	0.79	39.14	39.15	exp_2	pico	Immersed
40	41.19	0.58	41.19	41.20	exp_2	pico	Immersed
32	32.16	0.94	32.15	32.17	exp_2	apex	Immersed
34	34.10	0.22	34.09	34.11	exp_2	apex	Immersed
36	36.08	0.15	36.06	36.09	exp_2	apex	Immersed
38	38.08	0.16	38.06	38.10	exp_2	apex	Immersed
40	40.00	0.12	39.97	40.02	exp_2	apex	Immersed
32	31.46	1.94	31.46	31.46	exp_3	pico	Immersed
34	32.96	1.26	32.96	32.96	exp_3	pico	Immersed
36	34.41	1.97	34.41	34.42	exp_3	pico	Immersed
38	35.58	0.56	35.57	35.58	exp_3	pico	Immersed
40	38.89	1.36	38.89	38.89	exp_3	pico	Immersed
32	32.15	0.28	32.14	32.15	exp_3	apex	Immersed
34	34.12	0.29	34.11	34.12	exp_3	apex	Immersed
36	35.98	0.34	35.98	35.99	exp_3	apex	Immersed
38	37.99	0.16	37.98	38.00	exp_3	apex	Immersed

Treatment (°C)	Mean (°C)	SD (°C)	Lower CI	Upper CI	Experiment	Temperature Probe Source	Exposure
40	39.81	0.42	39.81	39.82	exp_3	apex	Immersed
32	NA	NA	32.58	32.59	exp_4	pico	Immersed
34	NA	NA	33.85	33.86	exp_4	pico	Immersed
36	NA	NA	35.75	35.77	exp_4	pico	Immersed
38	NA	NA	37.07	37.12	exp_4	pico	Immersed
40	NA	NA	39.05	39.10	exp_4	pico	Immersed
32	32.38	0.39	32.38	32.38	exp_4	apex	Immersed
34	34.25	0.37	34.25	34.25	exp_4	apex	Immersed
36	36.14	0.32	36.14	36.15	exp_4	apex	Immersed
38	37.95	0.29	37.93	37.96	exp_4	apex	Immersed
40	40.00	0.31	39.99	40.02	exp_4	apex	Immersed
32	32.02	0.34	31.98	32.05	exp_4	eb	Immersed
34	33.76	0.58	33.73	33.79	exp_4	eb	Immersed
36	35.20	0.94	35.17	35.23	exp_4	eb	Immersed
38	37.73	0.56	37.63	37.83	exp_4	eb	Immersed
40	37.57	0.98	37.47	37.67	exp_4	eb	Immersed
40	40.12	0.33	40.11	40.13	exp_5	elitech	Emersed
46	46.27	0.37	46.26	46.28	exp_5	elitech	Emersed
37	37.16	0.12	37.16	37.16	exp_6	elitech	Emersed
43	43.39	0.19	43.38	43.39	exp_6	elitech	Emersed
34	33.94	0.10	33.94	33.95	exp_7	elitech	Emersed
48	48.26	0.15	48.26	48.27	exp_7	elitech	Emersed

Experiment	Treatment (°C)	Mean Temperature (°C)	Mean DO (%)	SD DO (%)
exp_2	32	32.16	61.80	9.15
exp_2	34	34.10	51.05	14.26
exp_2	36	36.08	60.21	9.70
exp_2	38	38.08	53.56	4.78
exp_3	32	32.15	62.09	4.06
exp_3	34	34.12	38.15	3.32
exp_3	36	35.98	48.40	8.66
exp_3	38	37.99	36.93	26.79
exp_3	40	39.81	66.60	3.14
exp_4	32	32.38	49.30	7.79
exp_4	34	34.25	47.48	13.54
exp_4	36	36.14	49.32	6.11
exp_4	38	37.95	57.37	1.82
exp_4	40	40.00	51.07	10.48

Table S7: Summary statistics of dissolved oxygen (DO) across treatments in three of the five immersed experiments.

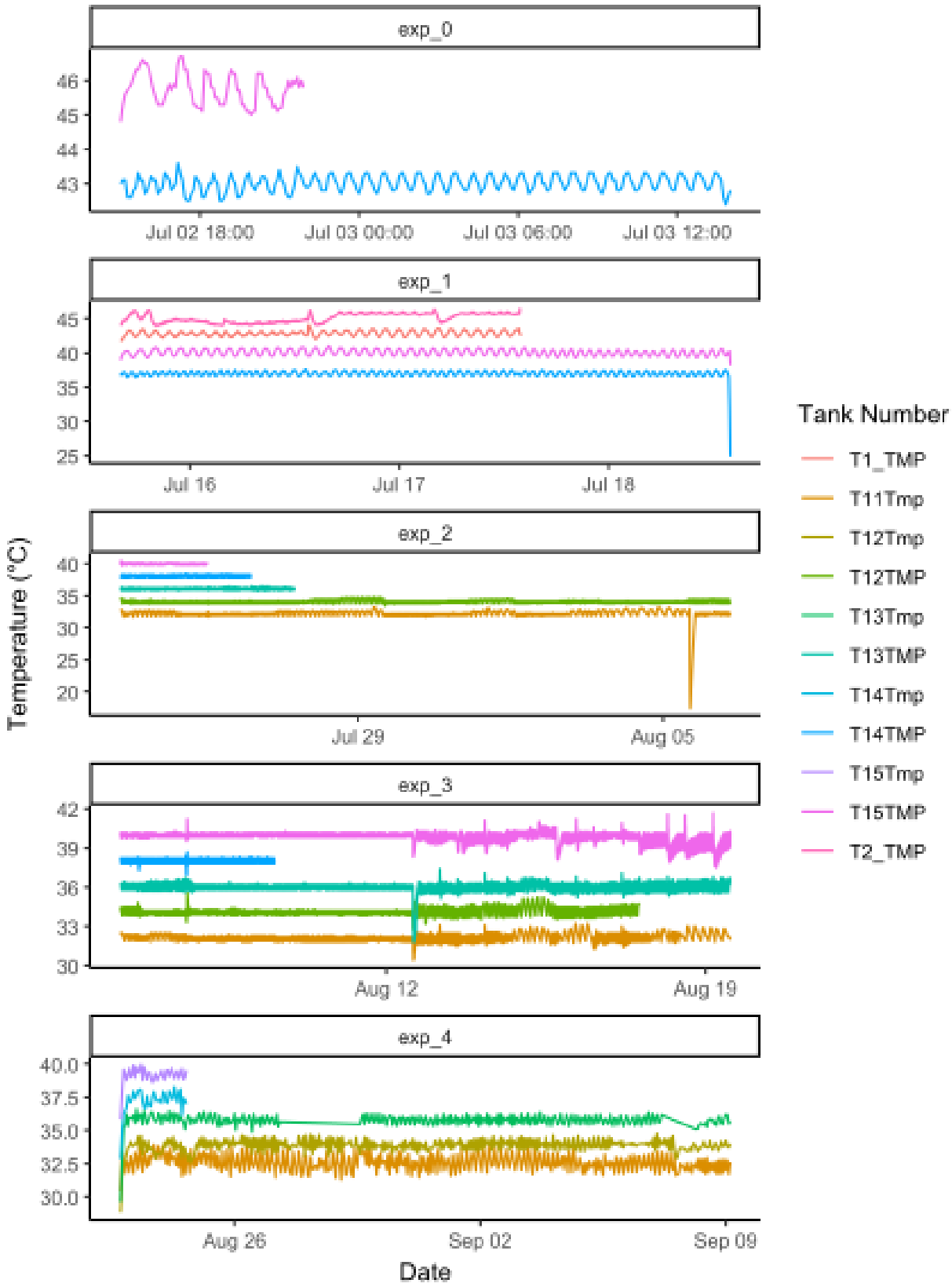

Figure S12: Temperature of immersed oysters during laboratory experiments. All temperatures were recorded using APEX seawater system probes except for experiment 4, where we used a separate thermocouple probe to measure water temperature. Length of time series for each tank is limited to amount of time any oyster was alive in that treatment.

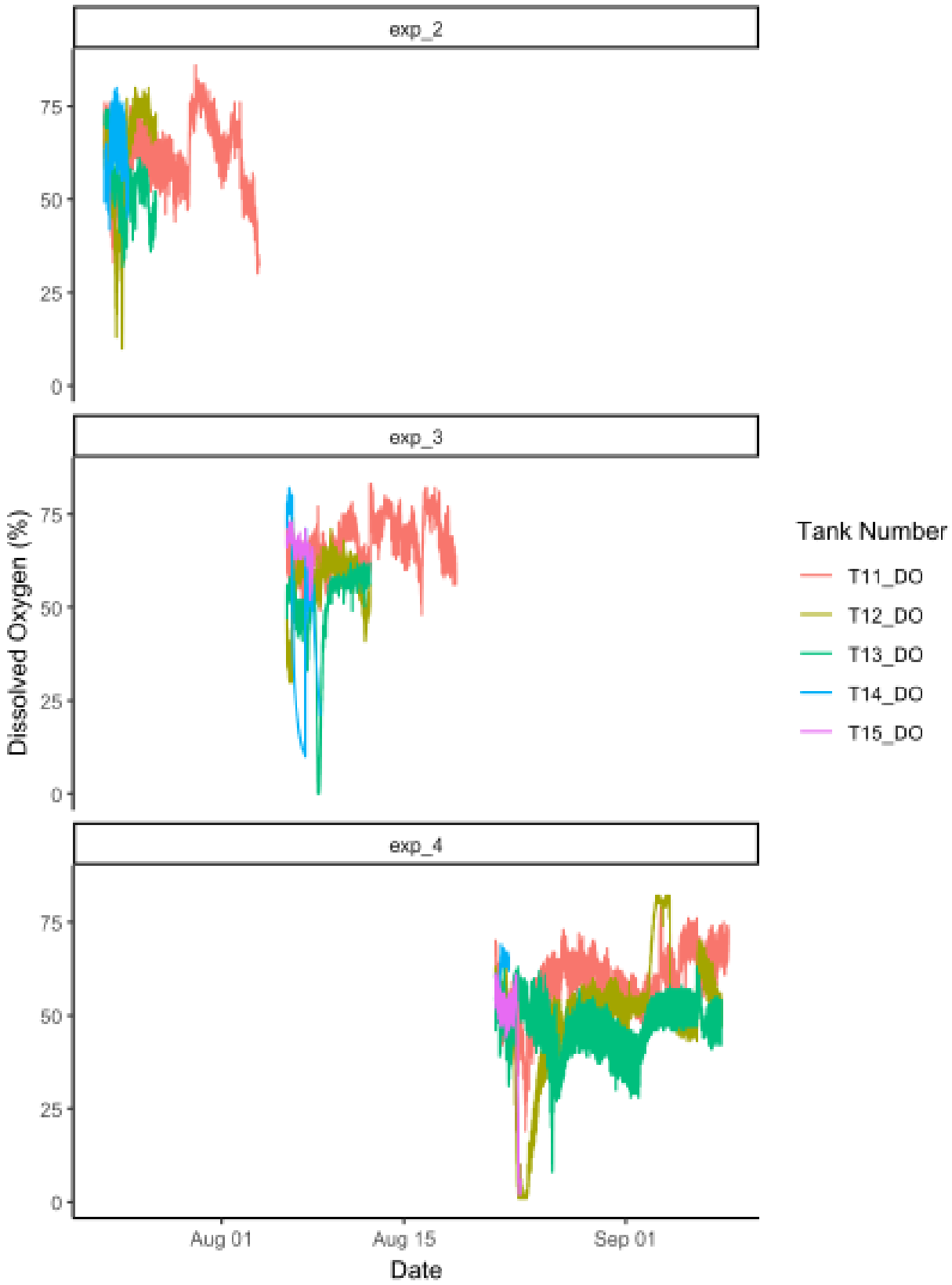

Figure S13: Dissolved Oxygen (DO) of immersed oysters during laboratory experiments. We only had access to oxygen probes during experiments 2, 3, and 4. Length of time series for each tank is limited to amount of time any oyster was alive in that treatment. However, because probes were placed in sub-tanks, it is possible that the oyster in the subtank with the probe died before the end of the presented time series.

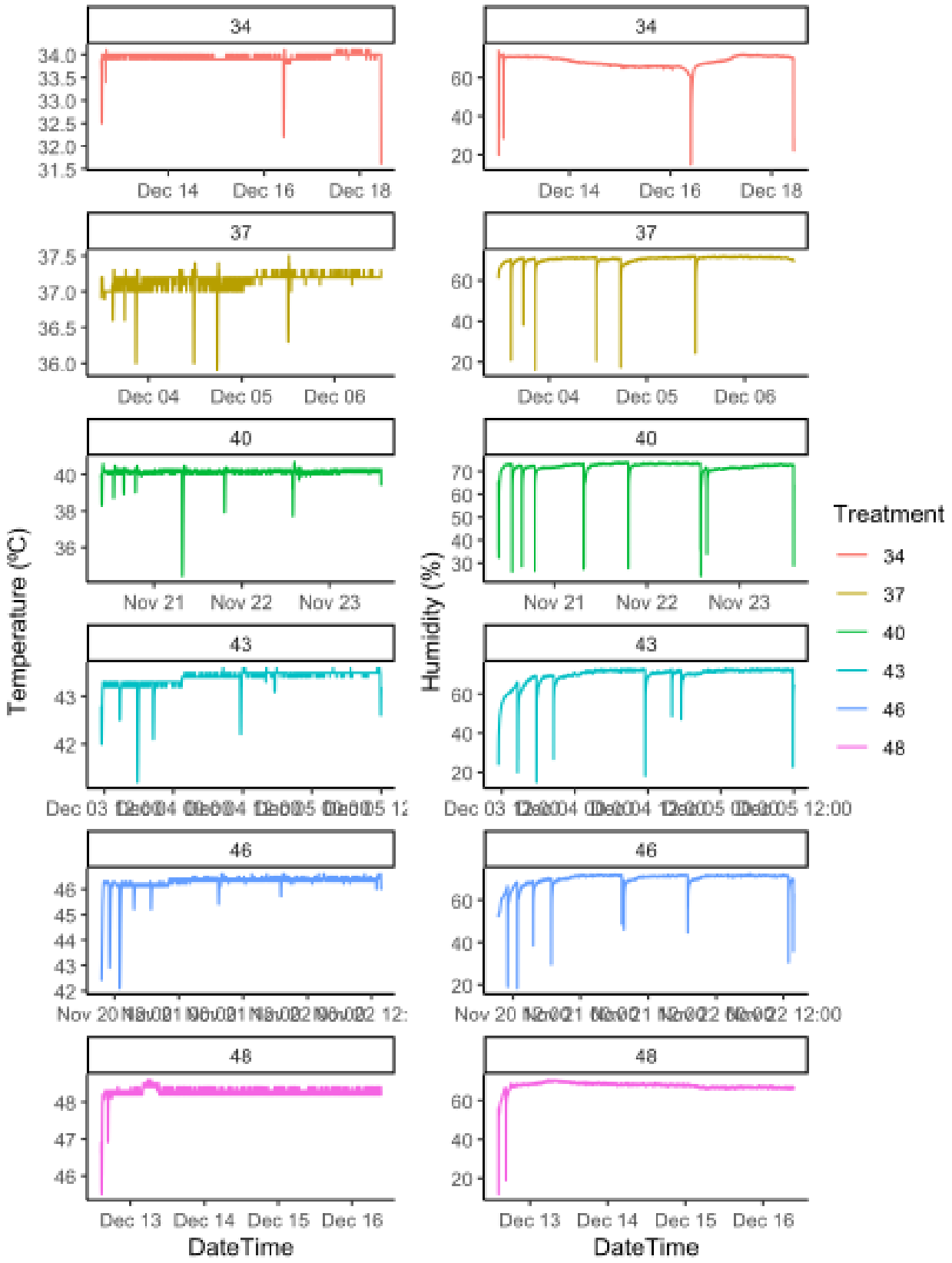

Figure S14: Humidity and temperature of emersed oysters during laboratory experiments. All data were recorded using Elitech data logger probes.

Figure S15: Caged oysters on pavers at Brackett's Point, NH.

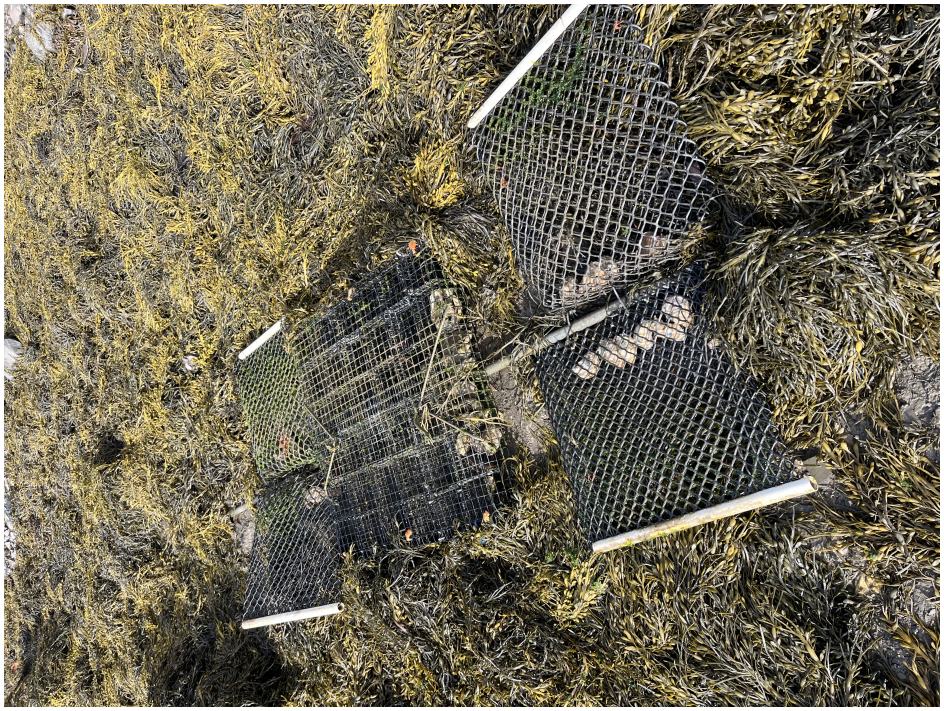

Figure S16: Caged oysters on pavers at Jackson Estuarine Lab (JEL), NH.

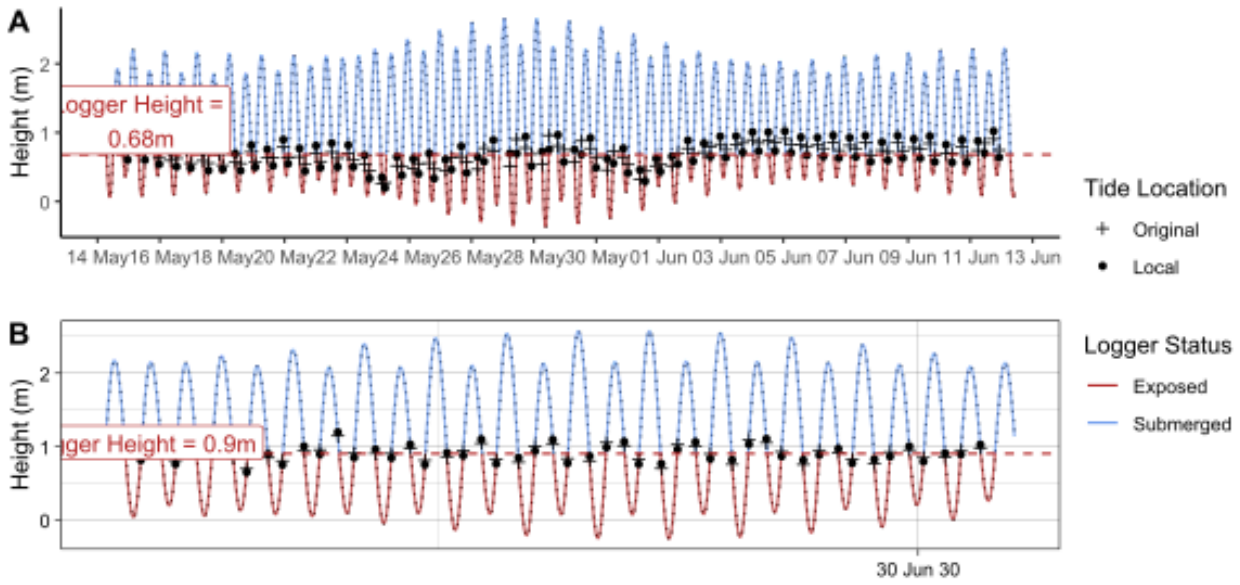

Figure S17: Tide series from Squamscott River showing calculated logger height from the `tide_heightfindR` function for both A) JEL and B) Brackett's Point. Original tide series is displayed as dotted line, time-shifted optimal tide series as the red and blue time series. Plusses indicate the tide height of immersion based on the unshifted tide series, while round points indicate the tide height of immersion based on the shifted time series. The blue parts of the tide series indicate timepoints where the tide is above the height of the logger (logger is underwater, submerged) while the red parts indicate when the tide is below the height of the logger (logger is exposed). Calculated tide height of the two oyster field deployments were 0.68 m (JEL) and 0.9 m (Brackett's Point) relative to MLLW

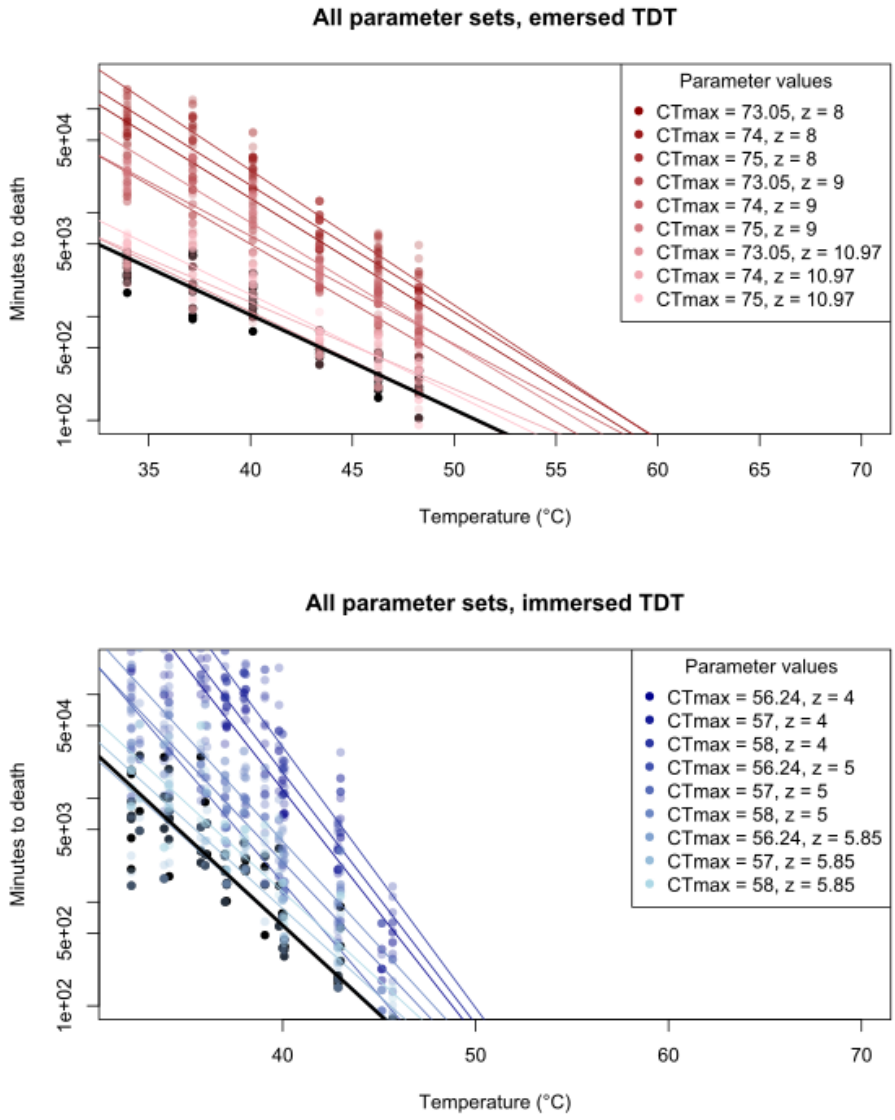

Figure S18: All 18 TDT curves used to build 18 unique emersed and immersed TTLs. $CT_{\max(1\,\min)}$ was either held constant or increased by 1 or 2°C, and z was either held constant or decreased by 1 or 2. All possible combinations of 9 emersed and 9 immersed TTLs result in 81 unique combinations we tested. Data were resimulated via a temperature-stratified residual bootstrap with replacement, with slope and intercept adjusted by the candidate $CT_{\max(1\,\min)}$ and z parameter pair.

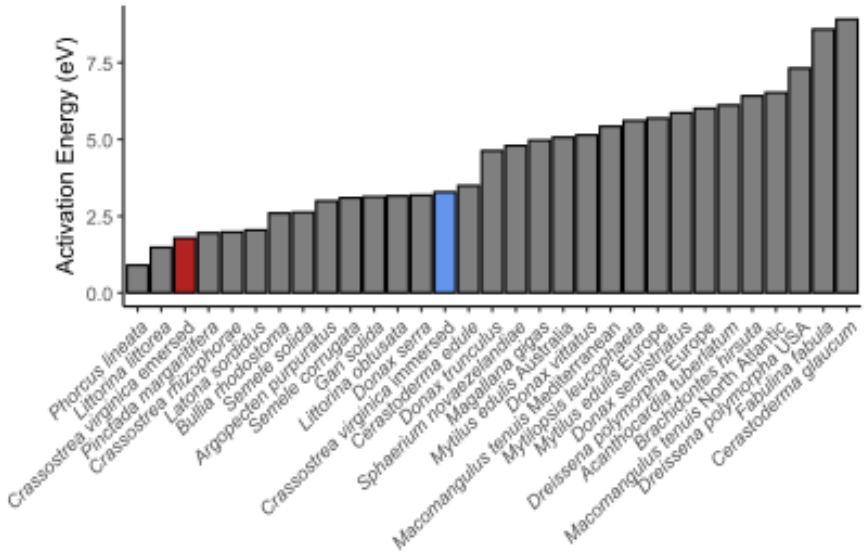

Figure S19: Activation energy (eV) of time to death (heat failure rate) across 31 aquatic and marine mollusks, with colored bars representing results from this paper's experiments. Data aggregated from (Jørgensen et al., 2022) and other sources.

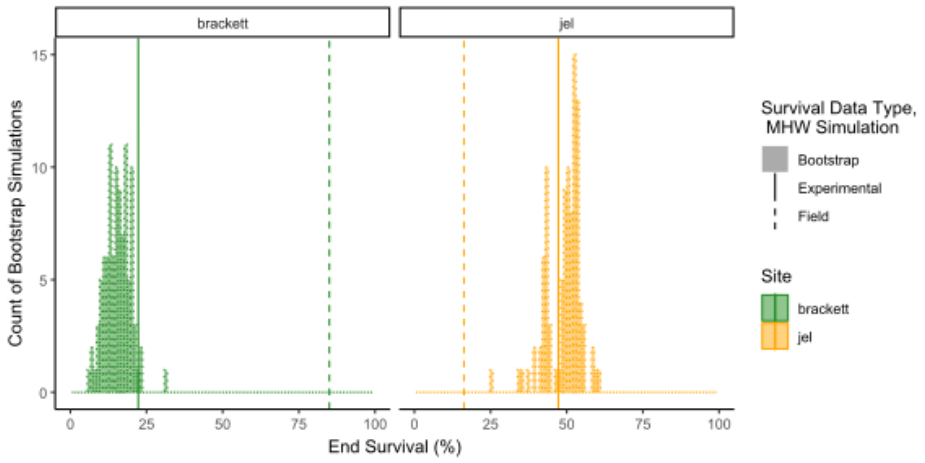

Figure S20: Histogram of bootstrapped minimum survival values at the end of each field deployment. Histogram bars represent the spread of survival data modeled after bootstrapping emersed and immersed TTLs in a dual-TTL model. Solid vertical lines represent the end modeled survival using the empirical TTL from laboratory experiments. Dashed vertical lines indicate the field observed survival values.

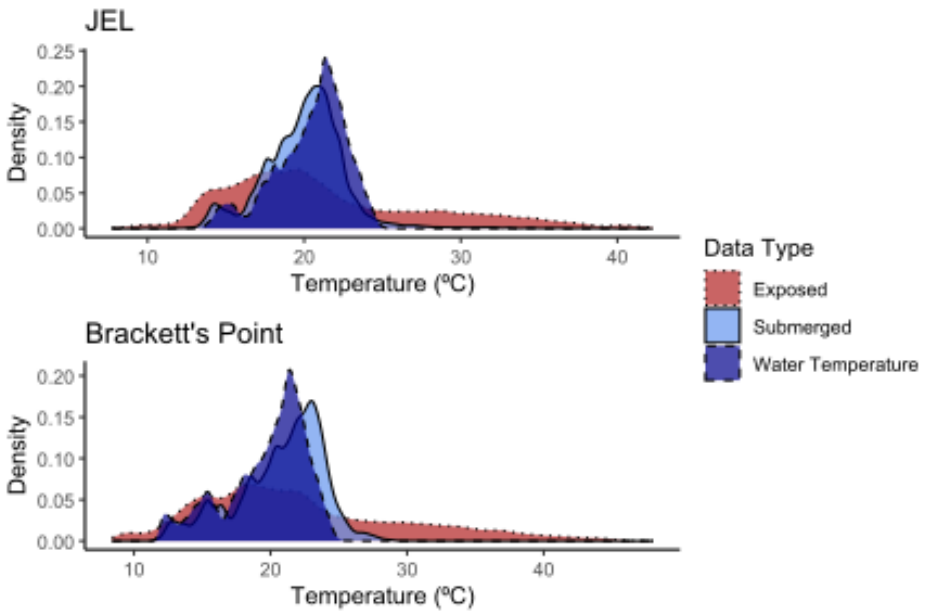

Figure S21: Density of observed intertidal and water temperatures across two deployment times in Great Bay, NH. Deployment 1 occurred between June 18th and August 28th, deployment 2 between July 18th and August 28th. Exposed and submerged water temperatures were identified from intertidal temperature logger time series based on the interpolated tide height of the logger. Water temperature was recorded over the same time period of each deployment from the nearby NERRS buoy GRBGBWQ.

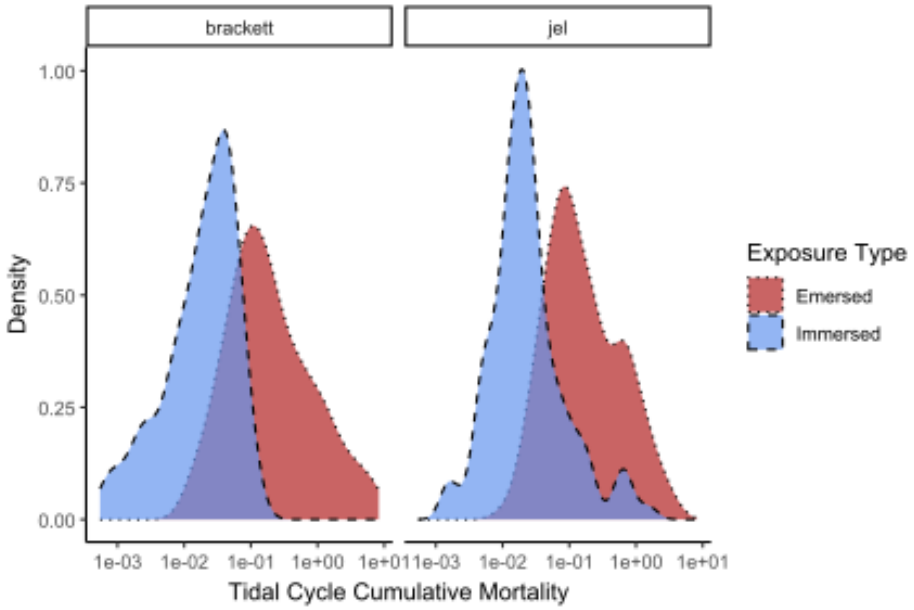

Figure S22: Density of cumulative mortality at the end of each tidal cycle for the combined-TTL model, attributed to immersion (high tide) and emersion (low tide) periods during each tidal cycle.

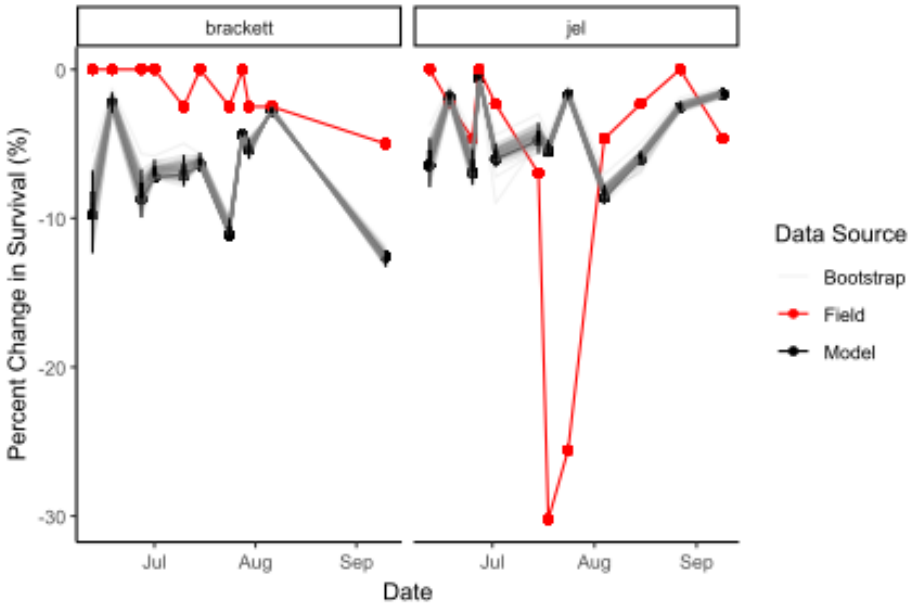

Figure S23: Percent change analysis of modeled and bootstrap data against field survival data. The change in survival between each field census date was calculated for field data (red), predicted survival (black), and bootstrapped survival estimates (gray)

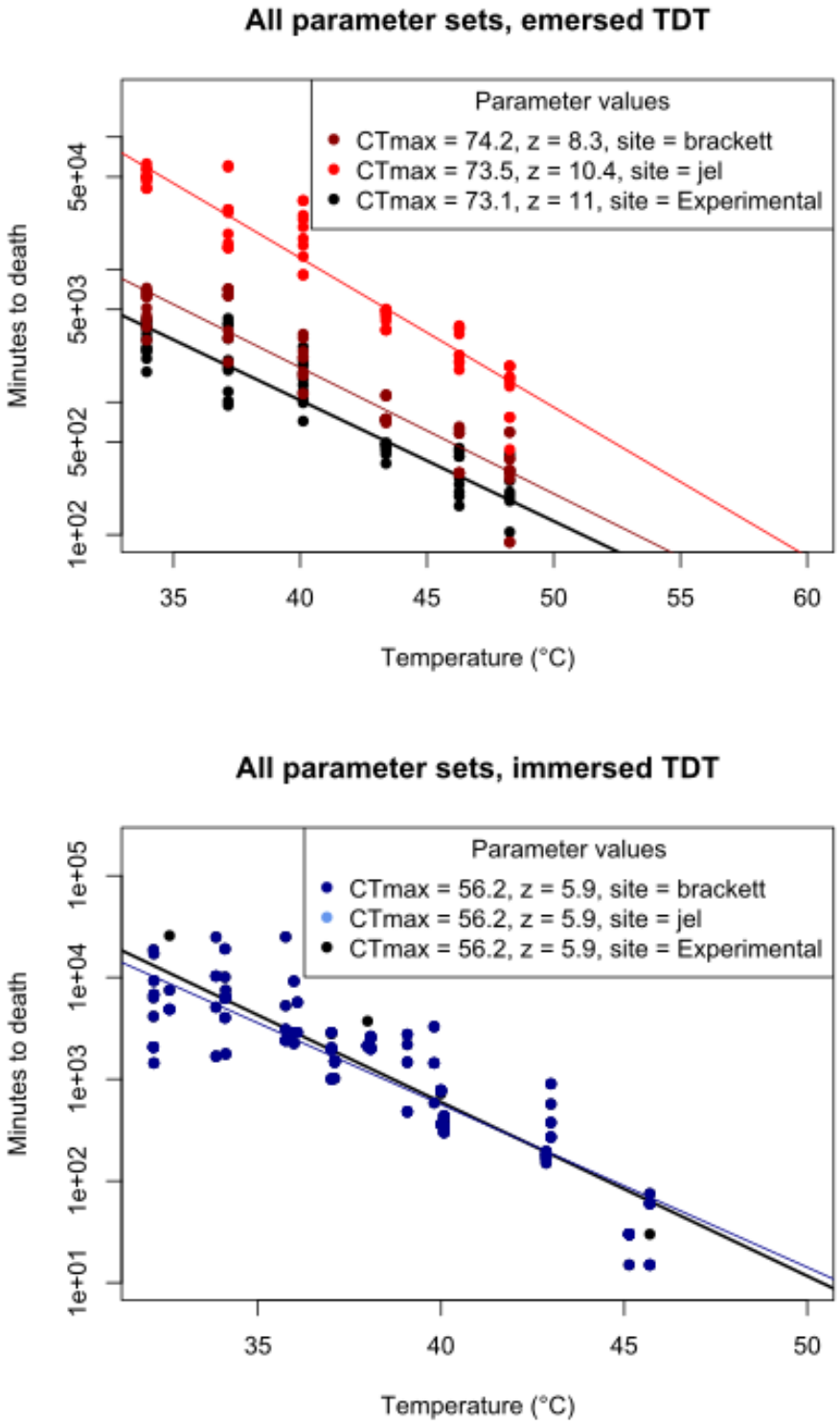

Figure S24: Optimal TDT curves based on percent change analysis between field collected oyster survival data and 81 candidate TTL parameter sets (18 candidate TTLs per immersed/emersed curve, all possible combinations).